

Review

Structure, Properties, and Preparation of MXene and the Application of Its Composites in Supercapacitors

Mingming Sun ^{1,*} , Wen Ye ¹, Jingyao Zhang ² and Kaining Zheng ²

¹ Basic Experimental Center for Natural Science, University of Science and Technology Beijing, Beijing 100083, China

² School of Advanced Engineering, University of Science and Technology Beijing, Beijing 100083, China

* Correspondence: sunmingming@ustb.edu.cn

Abstract: Two-dimensional transition metal carbides/nitrides (MXenes) are emerging members of the two-dimensional material family, obtained by removing the A layer of the MAX phase through methods such as liquid-phase etching. This article summarizes the structure and properties of MXenes, as well as several preparation methods, including etching with hydrofluoric acid and fluoride salts, alkali-based etching, electrochemical etching, Lewis acid molten salt etching, and direct synthesis. Due to their unique two-dimensional structure and surface chemistry, MXenes exhibit good metallic conductivity, hydrophilicity, excellent flexibility, and ion intercalation properties, showing great potential in the research and application of supercapacitors and attracting widespread attention. The combination of MXene with other types of materials, including polymers, metal hydroxides, metal oxides, and carbon materials, takes advantage of composites to improve energy storage performance and shows great potential in the research and application of supercapacitors. This article provides a detailed summary of MXene composite materials and capacitor performance and introduces the research progress of MXene materials in the field of supercapacitor energy storage applications, aiming to provide references for the preparation of high-performance MXene supercapacitor electrode materials.

Keywords: MXene; supercapacitor; composites; two-dimensional structure; transition metal carbides/nitrides



Citation: Sun, M.; Ye, W.; Zhang, J.; Zheng, K. Structure, Properties, and Preparation of MXene and the Application of Its Composites in Supercapacitors. *Inorganics* **2024**, *12*, 112. <https://doi.org/10.3390/inorganics12040112>

Academic Editors: Christian Julien and Qingguo Shao

Received: 12 March 2024

Revised: 3 April 2024

Accepted: 9 April 2024

Published: 12 April 2024



Copyright: © 2024 by the authors. Licensee MDPI, Basel, Switzerland. This article is an open access article distributed under the terms and conditions of the Creative Commons Attribution (CC BY) license (<https://creativecommons.org/licenses/by/4.0/>).

1. Introduction

The world economy is expanding at a rapid pace, and this has resulted in significant energy shortages and environmental degradation due to human overexploitation and the usage of non-renewable energy sources like coal and oil [1]. People have shifted more focus toward research on clean energy, but sustainable energy sources, including wind, hydropower, as well as solar energy, exhibit fluctuations and discontinuities in the production process. Equipment that stores energy with a high-energy density and outstanding stability of cycling is desperately needed, as the development of new energy devices, such as electric vehicles, is happening at a rapid pace. Advanced and efficient energy storage technologies are essential for the large-scale utilization of renewable energy, wearable electronic products, and electric vehicles. Supercapacitors, one of the most sophisticated energy storage technologies, have grown significantly in the last several years. The characteristics of the power density are high, the charging speed is fast, and the cycle life is long, making them widely applicable in consumer electronics, portable electronics, grid backup power, public transportation, and other fields [2]. The choice and application of electrode materials is one of the fundamental technologies in the study and creation of supercapacitors. In the future, high-energy, high-power-density supercapacitors will rely on substances that can accumulate charges by pseudocapacitance mechanisms or fast redox reactions. Thus, Consequently, enhanced supercapacitor electrode materials can benefit from the use of high-surface-area

two-dimensional (2D) materials [3–5]. Since the isolation of monolayer graphene in 2004, 2D materials have garnered wide attention due to the unique characteristics that they own compared to other volumetric forms. MXene is a new type of 2D carbonitride or transition metal carbide like graphene, possessing excellent conductivity and high redox activity. As an electrode material for supercapacitors, MXene holds broad application prospects [6–8].

MXene, a new member of the 2D materials family, was first synthesized by Gogotsi's group at Drexel University in the United States in 2011 [9]. They selectively etched aluminum from titanium carbide (Ti_3AlC_2) powder using hydrofluoric acid, obtaining two-dimensional layered carbide (Ti_3C_2) nanosheets. As the collective term for these novel 2D transition metal carbides, nitrides, and carbonitrides, MXene is only a few atoms thick [10–12]. MXene not only has the common properties of 2D materials but also exhibits superior characteristics to them: (1) the diversity of the M elements enables MXene to have a rich diversity of chemical compositions; (2) different preparation methods can be used to modulate the surface termination groups of MXene; (3) the significant energy level difference between M and X atoms and the effective use of surface termination groups enable the development of MXene with a metallic conductivity that surpasses that of even graphene; (4) the hydrogen bonding between water molecules and terminal groups gives MXene its hydrophilicity, as well as other characteristics [13–16]. Due to its versatile chemical properties and abundant surface modification space, MXene plays a crucial role in various technological applications such as storing energy, catalysis, sensors, electromagnetic interference shielding, and lubrication. MXene, as an electrode material, confers unique advantages to electrochemical energy storage devices and has attracted increasing attention; it is one of the current cutting-edge electrode materials for supercapacitors [17–20].

However, the problems of MXene's material agglomeration and accumulation, as well as the influence of its surface functional groups on the performance of capacitors, markedly limit the practical application of MXene materials. To improve energy storage performance, researchers have tried to compound MXene with other types of materials, including polymers, metal hydroxides, metal oxides, and carbon materials, leveraging the advantages of these composite materials. Therefore, many types of MXene composites have been derived which show excellent energy storage performance.

In this review, the crystal structures and properties of MXene materials are first introduced, as are several methods for preparing MXene materials, including hydrofluoric acid and fluorine salt etching, base etching, electrochemical etching, Lewis's acid molten salt etching, and direct synthesis. The types and properties of MXene composites include polymers, metal hydroxides, metal oxides, and carbon materials and are reviewed in detail. The progress of the research on MXene materials in the energy storage applications of supercapacitors is also introduced. Finally, the challenges and opportunities for MXene composites in the field of supercapacitors are discussed to provide a reference for the preparation and improvement of high-performance MXene electrode materials.

2. Structure and Properties of MXene

2.1. Structure of MXene

MXene is a two-dimensional layered material obtained by corroding the A layer of the precursor MAX phase by selection, leaving behind the M layer and X layer [21,22]. The MAX phase's chemical formula is $\text{M}_{n+1}\text{AX}_n$ ($n = 1, 2, 3$), in which M stands for early transition metal elements such as Ti, Zr, V, Nb, Cr, Mo, A mainly consists of group III and IV elements such as Al, Ga, In, and X indicates carbon and/or nitrogen elements [23–25]. After the corroding by selection of the A layer in the MAX phase, the material retains its inherent crystal structure by using a chemical formula of $\text{M}_{n+1}\text{X}_n\text{T}_x$ ($n = 1, 2, 3$), in which T represents surface functional groups like -OH, -O, and -F [26–28]. The schematic diagram of the MAX phase and MXene structure is shown in Figure 1 [29].

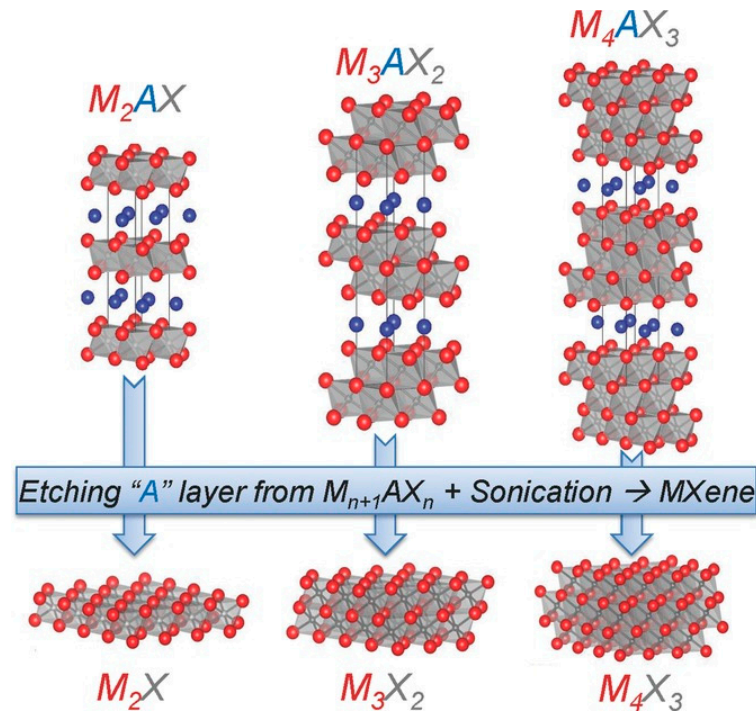


Figure 1. Structure of MAX phases and the corresponding MXenes. Reproduced with permission [29]. Copyright 2013, John Wiley and Sons.

Surface studies of MXene have shown that after removing the A layer, surface functional groups such as -OH and -F appear on the MXene surface [30,31]. By using density functional theory (DFT) calculations, Tang et al. discovered three possible configurations of surface functional groups (including -OH and -F) oriented in $\text{Ti}_3\text{C}_2\text{T}_x$, as shown in Figure 2 [32]. Each Ti_3C_2 monolayer consists of a five-layer stacking of Ti(1)-C-Ti(2)-C-Ti(1). All of them can be considered as a Ti_6C octahedron with edge-sharing shaped by three Ti atomic layers alternating with two C atomic layers (Figure 1). In the type I structure (Figure 2b,e), the surface functional groups -F and -OH are located above the vacancies of three neighboring carbon atoms, while in the type II structure (Figure 2c,f), the surface functional groups -OH and -F are located above the top carbon atom. The structure of type III (Figure 2d,g) is formed by the mixture of type I and type II, with the surface functional groups situated in the hollow site on one side as the type I structure and on the carbon atom on the other side as the type II structure. Comparing the relative DFT total energies, it was found that their structural stability followed the rule of $\text{I} > \text{III} > \text{II}$, indicating that F and OH functional groups lean toward adopting the type I configuration.

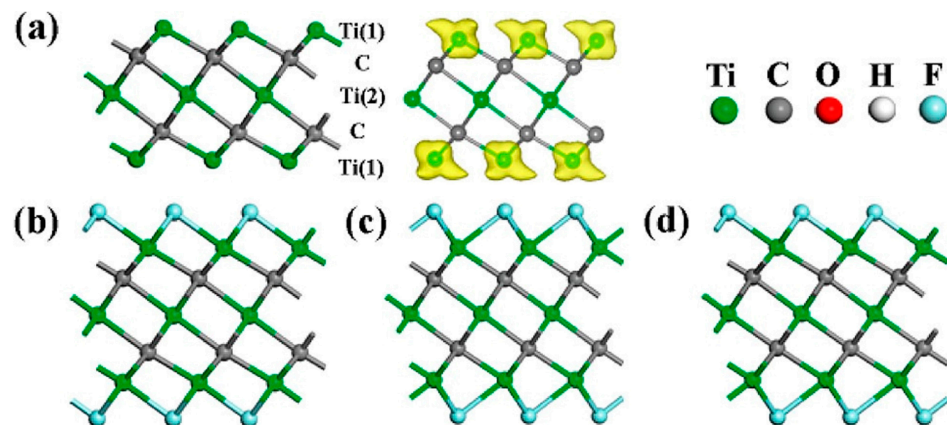


Figure 2. Cont.

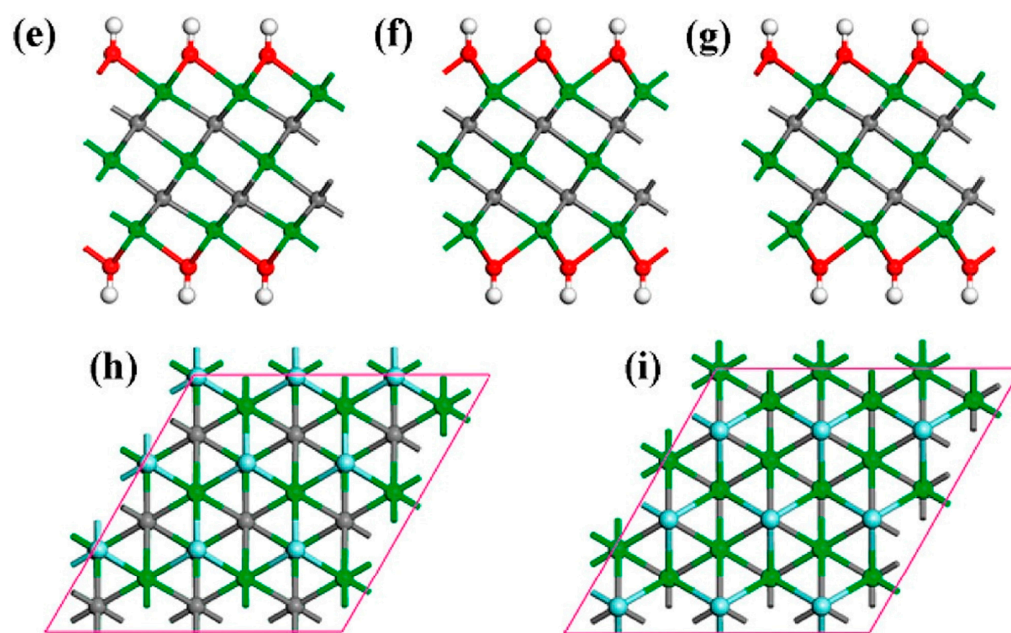


Figure 2. Optimized the free-standing Ti_3C_2 monolayer's geometries and its fluorinated and hydroxylated structural forms: (a) a quintuple layer with Ti(1)-C-Ti(2)-C-Ti(1) stacking modes is shown in side views (left), and the bare Ti_3C_2 monolayer is generated by the computed spin density distribution (middle); side views of (b) I- $\text{Ti}_3\text{C}_2\text{F}_2$, (c) II- $\text{Ti}_3\text{C}_2\text{F}_2$, (d) III- $\text{Ti}_3\text{C}_2\text{F}_2$, (e) I- $\text{Ti}_3\text{C}_2(\text{OH})_2$, (f) II- $\text{Ti}_3\text{C}_2(\text{OH})_2$, and (g) III- $\text{Ti}_3\text{C}_2(\text{OH})_2$; (h,i) the top views of I- $\text{Ti}_3\text{C}_2\text{F}_2$ and II- $\text{Ti}_3\text{C}_2\text{F}_2$. Reproduced with permission [32]. Copyright 2012, American Chemical Society.

2.2. Properties of MXene

2.2.1. Capacitive Properties

MXene has rich oxidation-reduction sites, which leads to high capacitance [33,34]. Taking $\text{Ti}_3\text{C}_2\text{T}_x$ MXene as an example, Ti's oxidation state continuously changes owing to the hydration of the oxygen-containing terminal groups, providing charge transfer capability for the valence transition metal [35,36]. The end groups on the surface of MXene also play a key role in energy storage [37]. Generally speaking, =O functional groups are more stable than -OH and -F because they share more electrons with the M element in the MXene layer, and the conversion between the =O and -OH end groups during charge and discharge processes provides a large number of active sites for redox reactions [38,39]. The unique layered structure of 2D MXene means a larger surface area, and the multi-layered structure is more conducive to ion intercalation and transmission [40]. Supercapacitors made from MXene have excellent volumetric capacitance (about 1500 F cm^{-3}) [34,41]. In addition, the layered structure of MXene allows it to adapt to various intercalating agents, which helps to expand the electrochemical reaction activity of MXene compared to the surface area, enhancing pseudocapacitance and cycling stability [42,43]. The good energy storage capacity of MXene is reflected in the devices fabricated with it, which have high energy and power densities.

2.2.2. Conductivity

MXenes have excellent conductivity, with a metallic conductivity of up to $\sim 24,000 \text{ S cm}^{-1}$. The structure of MXene contains many transition metal elements, for example, titanium and molybdenum, which usually have high conductivity, forming conductive channels in the MXene structure and promoting electron transmission [44–46], thereby improving the overall conductivity of MXene [47–49]. MXene is a 2D material with a large specific surface area, which means higher electron accessibility. Electrons can freely transmit on the 2D plane, reducing electron scattering losses and improving conductivity performance. The morphology of MXene also has a great impact on its conductivity; single-layer and

large-sized flakes have better interaction than multi-layered and small-sized flakes, usually improving conductivity [14,50,51]. In addition, compared with other 2D materials such as metal sulfides/hydroxides or graphene, MXene has plenty of chemical functional groups, for example, hydroxyl and fluorine atoms, and by changing these functional groups, the electronic structure and charge transfer properties of MXene can be controlled, affecting its conductivity performance [52]. Overall, the improvement of MXene conductivity is mainly due to its unique structure, containing transition metal elements and abundant chemical functional groups, which together make MXene an excellent conductive material with a multitude of potential applications. The MXene's excellent conductivity ensures rapid electron transmission, making it possible to achieve high-power density supercapacitors. In the manufacturing process of electrodes, conductive agents and current collectors are not even necessary, which helps to improve the energy density of the entire device [53,54].

2.2.3. Hydrophilicity

MXene has good hydrophilicity mainly due to the abundant oxygen, hydrogen, and other functional groups in its layered structure, including -OH, -F, etc., making the MXene surface highly polar [55–57]. In water, these polar functional groups can form hydrogen bonds and other interaction forces with water molecules, causing attractive forces between MXene particles and water molecules, showing excellent hydrophilicity [58]. What's more, the interlayer structure of MXene contains lots of hydrogen bond acceptors, contributing to forming hydrogen bonds with water molecules, which also increases its compatibility with water [59]. Furthermore, the hydrophilicity of MXene can be improved due to its characteristics such as the porous structure and high specific surface area, because these characteristics can help to expand the contact surface area between MXene and water, and the mutual interaction with water can also be improved as well [60]. To summarize, the superior hydrophilicity of MXene is gained due to its features, including the abundant polar functional groups, hydrogen bond sites, porous structure, high specific surface area, and the layered structure of MXene. This property equips MXene with excellent dispersion, stability, as well as application potential in water-based systems, preparing for its widely used application in water-based supercapacitors and other fields [61,62].

2.2.4. Mechanical Flexibility

The layered structure of MXene is critical to its flexibility in the sphere of mechanics. MXene consists of numerous layers of 2D nanosheets, which are put on top of each other via relaxed bonding. The function of the 2D nanosheets is that they allow MXene to slide and shear under forces that are produced by external objects, which also gives MXene great deformability and ability to bend [63]. Meanwhile, through the method of intercalating other materials (like polymers or liquids), the MXene's layered structure can be greatly improved to form composite materials, as well as enhance its flexibility [64,65]. Chu et al. synthesized two-dimensional transition metal carbide/polyimide ($\text{Ti}_3\text{C}_2\text{T}_x$ MXene/PI) films through in situ polymerization and a simple scratch method, which showed enhanced flexibility. It can better adapt to the deformation of the capacitor, which is conducive to improving the contact efficiency between the electrode and the electrolyte of the capacitor, thus improving the performance [66]. M-Xenes' mechanical characteristics are decided by their structural combination, size, defects, density, incomplete nanosheet edges, surface end groups, and M-X elements. Like other 2D materials, each thin sheet determines its inner mechanical properties [67]. The surface end groups are essential for improving the mechanical characteristics of M-Xenes. For instance, =O end groups can strengthen the M-Xenes' interlayer attraction. And it can also improve the M-Xenes' resistance to shear and strain. The high-specific surface area and mesoporous structures can also enhance the flexibility of M-Xenes materials. Through applied high-specific area and mesoporous structures, the contract surface and external environment can be increased, and the stress concentration can be reduced, which can provide more and more displacement and deformation space and enhance M-Xene's flexibility and durability, which reduce

the influence of external vibration on the internal structure of the capacitor. Furthermore, according to a study by Guo et al., under uniaxial and biaxial conditions, respectively, upon the addition of =O end groups, the results have shown that the tensile range of Ti_2C was increased to 28% and 20%, which indicates the inhibitory influence of surface terminal groups on Ti_2C 's collapse [68]. Therefore, the addition of =O end groups of Ti_2C can prevent the capacitor from being easily damaged when bending or stretching to maintain stable performance. In conclusion, the mechanical flexibility of M-Xenes material originates from its high specific area, layer structure, mesoporous structure, and chemical composition. Therefore, M-Xenes has a wide range of potential applications. It also is the source of inspiration for the new materials to become reliable and flexible. Sun et al. modulated size refinement to decrease the grain size, introducing more grain boundaries, which stopped dislocations and crack propagation under deformation. This resulted in increased strength and toughness. The MXene with the size refinement showed increased energy density and power density of the supercapacitors [69,70]. Mechanical performance will affect the electrode's electrochemical performance, especially in future applications, where the electrode of flexible electronic devices will be subjected to stress, bending, and twisting. To this end, we summarize the relative advantages of mechanical flexibility of MXene and other kinds of two-dimensional materials at Table 1. MXene has excellent mechanical flexibility, which helps to maintain good electrochemical performance and facilitates its application in flexible supercapacitors and micro-supercapacitors [71].

Table 1. Comparison of mechanical flexibility of MXene with other 2D materials.

Property	MXene	2D Carbon Nitride Material	2D Transition Metal Dichalcogenides	Clay-Type 2D Material
	Very high	Low	Moderate	Moderate
Flexibility	Excellent flexibility, maintains stability during bending	Relatively prone to deformation during bending	Tends to lose stability during bending	Prone to fracture during bending
	Excellent	Normal	Poor	Poor
Elastic Recovery	Demonstrates excellent elastic recovery ability	Normal elastic recovery under stress	Poor elastic recovery under stress	Significant deformation under stress
	Outstanding	Normal	Normal	Poor
Tensile Strength	Demonstrates excellent resistance to fracture	Displays ordinary performance during stretching	Susceptible to structural damage during stretching	Susceptible to rupture during stretching
	Excellent	Normal	Normal	Poor
Post-Bending Recovery Performance	Rapidly recovers to original performance after bending	Slow recovery of performance after bending	Limited recovery of performance after bending	Incomplete recovery of performance after bending
	Outstanding	Normal	Normal	Poor
Fatigue Resistance	Demonstrates outstanding fatigue resistance, maintaining high performance over extended periods of stress	Normal fatigue resistance, prolonged stress affects performance	Moderate fatigue resistance, performance diminishes over time under stress	Poor fatigue resistance, prone to fatigue failure

3. Preparation of MXene

Typically, through the selective removal of atomic layers, MXenes can be synthesized (for example, Al, Si, Ga, or Sn) from the MAX phase using different methods. When the metal-metallic M–A bonds in MAX materials are less powerful than the M–X covalent bonds, selective etching of the A layer atoms from MAX can be achieved, and it will not

break the M–X bonds [18,33,52,59]. Currently, MXenes are produced by wet-chemical etching using HF or HF-containing or HF-generating etchants, resulting in the presence of -F surface terminations [45,72–74].

3.1. Etching Methods Based on HF and Fluoride Salts

When using HF as an etchant, elements A and M have strong chemical bonds, and the parent phase material will be destroyed. Mashtalir et al. [72] examined the dynamic control course of selective corroding of Al from Ti_3AlC_2 in 50% (mass fraction) HF and showed how the fast phase transition from bulk Ti_3AlC_2 to $\text{Ti}_3\text{C}_2\text{T}_x$ is facilitated by raising the sinking temperature, lengthening the reaction time as well as lowering the initial maximum particle size while confirming exfoliated single-layer $\text{Ti}_3\text{C}_2\text{T}_x$ MXene can exist under HF etching. Wang et al. [73] the synthesis of $\text{Ti}_3\text{C}_2\text{T}_x$ MXene from Ti_3AlC_2 powder by using 50% HF at room temperature, leading to the existence of -OH or -F surface groups on the surface and edges of MXene, and the accordion-like morphology obtained after HF treatment. At the atomic level, after HF modification, it was proven that the functional groups of MXene could be arranged in the Ti atoms' top position, as shown in Figure 3a. Additionally, as an etchant, HF lends itself toward the preparation of $\text{Ti}_3\text{C}_2\text{T}_x$ flakes with comparatively small lateral dimensions and multiple drawbacks. The use of HF etching is a convenient and universal method for preparing MXene, but HF is highly toxic and dangerous, and the synthesized MXene may contain a number of defects. It was discovered that HF synthesized in situ from a combination of salts, including fluoride (LiF, NaF, CaF_2 , etc.) and acids (HCl, H_2SO_4) has a similar etching behavior to pure HF but is much milder, while the obtained MXene flakes have larger lateral dimensions without the frequent observation of nanoscale defects, as seen in HF-etched samples [72]. By etching in a LiF + HCl solution, Ghidui et al. [6] obtained $\text{Ti}_3\text{C}_2\text{T}_x$ MXene, which had a lattice parameter of 2.7~2.8 nm, while the corresponding value for $\text{Ti}_3\text{C}_2\text{T}_x$ etched using HF is 2.0 nm. It is thought that LiF + HCl corrosion can produce larger interlayer spacing, which creates much more electrochemically active surfaces and quicker electrolyte ion diffusion channels. Additionally, similarly, mild etchants with little harm to the human body include NH_4HF_2 , which generates HF in situ on the precursor surface [74]. When dissolving the fluoride salt in an HCl solution, HF will be formed in situ. Cations (such as Li^+ and NH_4^+) can be used as intercalants to produce $\text{Ti}_3\text{C}_2\text{T}_x$ MXene flakes without Al layers and with increased interlayer spacing. In the synthesis process, etching and exfoliation occur simultaneously. Using the Minimally Invasive Layer Delamination (MILD) technique, HF can be generated in situ by reacting LiF with HCl. This method has potential applications and advantages in MXene synthesis. Firstly, the MILD technique is safer than direct HF usage as it controls the generation of HF, thereby reducing operational risks. Secondly, the MILD method may result in more uniform and controllable layer delamination, facilitating the production of high-quality MXene materials. Additionally, precise control over MXene's structure and properties can be achieved by adjusting the reaction conditions, thus expanding its potential applications in fields such as energy storage, catalysis, and sensing. Therefore, the introduction and further investigation of the MILD technique in the synthesis of MXene are of considerable importance and offer more sustainable and safer solutions for the preparation and application of MXene materials.

3.2. Alkali-Based Etching Method

To avoid damaging biological tissues due to the use of HF and fluoride salts, new synthetic methods have been explored. Alkali and Al elements have a strong binding affinity, and it is theoretically feasible to use an alkali-based etching method to synthesize MXene from MAX phases. Therefore, an alkali-based etching method can be adapted to synthesize MXene from MAX phases. Xie et al. [75] treated $\text{Ti}_3\text{C}_2\text{T}_x$ powder in 1 mol/L NaOH solution. Then added, 1 mol/L H_2SO_4 at 80 °C for 2 h to obtain $\text{Ti}_3\text{C}_2\text{T}_x$ MXene. Li et al. [76] created Ti_3AlC_2 in the presence of a small quantity of water and KOH and discovered that -OH groups take the place of the Al layers in the structure of Ti_3AlC_2 during

the etching process. The etching destroys the particle shape derived from the precursor of Ti_3AlC_2 , and randomly stacked nanosheets are combined with some scattered nanosheets, as shown in Figure 3b. Completely layered $\text{Ti}_3\text{C}_2(\text{OH})_2$ nanosheets can be effectively obtained via a simple washing process. KOH acts as a fluoride etchant to remove the Al layer more safely. The results show that materials prepared without fluoride functional groups have better energy storage performance compared to those prepared using the HF etching method. Because the pressure reaches 106 Pa and the water vapor is below $180\text{ }^\circ\text{C}$, this strategy was later used to manufacture 2D $\text{Ti}_3\text{C}_2(\text{OH})_2$ nanoribbons [77]. Li et al. [78] successfully prepared high-purity multilayer MXene without fluoride at $270\text{ }^\circ\text{C}$ in a 27.5 mol/L NaOH solution. Here, the dissolution of Al layers in NaOH yielded soluble $\text{Al}(\text{OH})_4^-$. The reaction temperature is an essential component of the continual etching of Ti_3AlC_2 , and the concentration of NaOH affects the mass fraction of the resulting MXene. They prepared a powder with a mass fraction of surface groups containing -OH and -O that reached 92%. Non-fluorinated functional groups and cation intercalation result in larger interlayer distances [79], demonstrating an increased capacity and improved rate performance compared to $\text{Ti}_3\text{C}_2\text{T}_x$ produced using the HF etching method. This preparation method requires a high-concentration and high-temperature alkali and is relatively risky, and thus is currently limited to the preparation of $\text{Ti}_3\text{C}_2\text{T}_x$; however, this non-fluorinated MXene is beneficial for optimizing the energy storage performance of supercapacitor.

3.3. Electrochemical Etching Method

The etching methods that have been mentioned involve fluorine-containing reagents or high-concentration alkalis and operate under relatively harsh conditions of high temperature and high pressure, with inherent dangers and limitations. From this perspective, electrochemical etching is a milder method. Etching in a non-fluoride electrolyte through the application of a constant potential can selectively etch the Al layer, where chloride ions (Cl^-) have great characteristics of easy combination with Al. Also, it can break the Ti-Al connection to form $\text{Ti}_3\text{C}_2\text{T}_x$ MXene with no terminal fluorine. Specifically, when the Ti_3AlC_2 electrode carries a positive charge, the erosion of Cl^- causes the forming of AlCl_3 and termination of the Ti atoms on the edge with chlorides, followed by the opening of grain boundaries to facilitate deeper action of Cl when it infiltrates and penetrates- and action of other substances when it intercalates in the electrolyte. Yang et al. [80] stated that an efficient electrochemical etching method relied on an anodic corrosion process to strip Ti_3AlC_2 . The electrolyte used is a mixture of 1.0 mol/L NH_4Cl and 0.2 mol/L TMAOH, with a pH value greater than 9. During the corroding process, as Cl^- has a strong binding affinity with Al, it breaks the Ti-Al bond and forms $\text{Ti}_3\text{C}_2\text{T}_x$ materials (Figure 3c). Furthermore, the intercalation of NH_4OH opens the edge etching of Ti_3AlC_2 , promoting deep etching below the surface. Pang et al. [81] examined a commonly used Ti-based method for synthesizing MXenes: thermally facilitated electrochemical etching in diluted hydrochloric acid solution.

3.4. Lewis Acid Molten Salt Corroding Method

Aside from the above corroding strategies, there are also methods to remove A-layer atoms from MAX phases in molten salts [18,53]. In 2019, Li et al. [82] obtained Ti_3ZnC_2 MAX phase from Ti_3AlC_2 and ZnCl_2 Lewis acidic molten salt through a displacement reaction at $550\text{ }^\circ\text{C}$. Increasing the ratio of MAX: ZnCl_2 , Ti_3ZnC_2 can be further converted into $\text{Ti}_3\text{C}_2\text{Cl}_2$ MXene. In 2020, Li et al. [83] etched a Ti_3AlC_2 MAX phase in molten ZnCl_2 while other Lewis acidic molten salts at temperatures over $500\text{ }^\circ\text{C}$ were used to produce $\text{Ti}_3\text{C}_2\text{Cl}_2$ MXene with chlorine (-Cl) surface terminations, eliminating unnecessary hydrolysis and oxidation in the MAX etching of molten salt (Figure 3d). The Talapin group [84] synthesized various MXenes with -Cl surface terminations in CdCl_2 molten salt and prepared several MXenes with Br surface terminations using Lewis acidic CdBr_2 , extending the molten salt etching pathway beyond chlorides.

3.5. Direct Synthesis Method

In comparison to the strategy of selectively removing A-layer atoms from MAX to extract MXene through the chemical etching mentioned above, researchers have also explored the use of chemical vapor deposition (CVD) to prepare MXene [85]. The research group of Dmitri V. Talapin at the University of Chicago reported a method for directly synthesizing MXene without the need to prepare the MAX phase and then perform etching [86]. They first attempted traditional solid-state synthesis by heating a stoichiometric mixture of solid precursors until the desired phase was formed. Subsequently, they developed a chemical vapor deposition (CVD) method. They used metal Ti, titanium chloride (TiCl_3 or TiCl_4), and a carbon source or nitrogen source (including graphite, CH_4 , N_2) as precursors to prepare various MXenes, including the widely used MXene- Ti_2CCl_2 (Figure 3e), as well as MXenes that had not been synthesized from MAX phase before. Using the CVD method, MXenes with carpet-like structures and complex spherical morphologies have been grown. This new direct synthesis method saves time, avoids the generation of hazardous waste related to the etching step, improves the efficiency of MXene preparation, and is expected to accelerate the industrial applications of these materials.

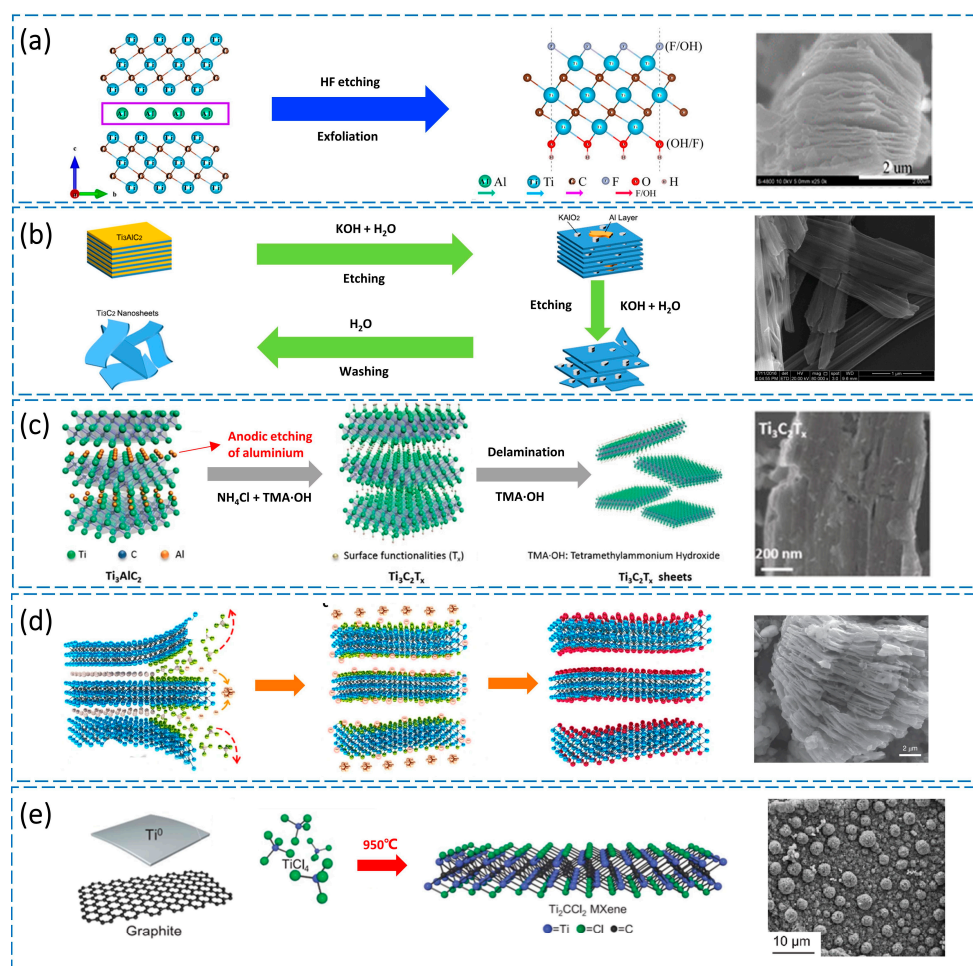


Figure 3. (a) Synthesis and SEM of $\text{Ti}_3\text{C}_2\text{T}_x$. Reproduced with permission [73]. Copyright 2015, American Chemical Society. (b) Schematic illustration of the etching process and SEM for Ti_3AlC_2 . Reproduced with permission [76]. Copyright 2017, American Chemical Society. (c) Schematic of the etching process and SEM for Ti_3AlC_x . Reproduced with permission [80]. Copyright 2017, Angewandte Chemie International Edition. (d) The reaction between Ti_3SiC_2 and CuCl_2 results in the formation of $\text{Ti}_3\text{C}_2\text{T}_x$ MXene and SEM. Reproduced with permission [83]. Copyright 2020, Nature Materials. (e) Schematic diagram of the direct synthesis and SEM of Ti_2CCl_2 MXene. Reproduced with permission [86]. Copyright 2023, American Chemical Society.

4. Application of MXene-Based Composite Materials in Supercapacitors

After the emergence of MXene, extensive research has been conducted on its electrochemical properties [87,88]. Ion intercalation is made by the open interlayer space in MXene's layered structure of stacked nanosheets, thereby storing charge. The MXene surface can form an electric double layer (EDL), serving a similar function. In an aqueous electrolyte solution, the MXene electrode's CV curve exhibits a rectangular shape, which is a typical characteristic of EDL capacitors [89]. In an aqueous electrolyte solution, hydrated cations (such as Li^+) intercalate into the interlayers without dehydration. Due to the inability of the isolated atomic orbitals of cations in the hydration shell to hybridize with the orbitals of MXene, an internal potential difference is produced by separated positive and negative charges: $\Delta\varphi = \varphi_e E - \varphi_i E$ (where $\varphi_e E$ and $\varphi_i E$ are the internal potentials of electrons and ions in the electrode), constituting an EDL in the interlayer space. Lukatskaya et al. [90] first illustrated the spontaneous insertion of cations from saline solutions between the layers of $\text{Ti}_3\text{C}_2\text{T}_x$ MXene, such as Na^+ , K^+ , NH_4^+ , Mg^{2+} , and Al^{3+} . In KOH solution, binder-free $\text{Ti}_3\text{C}_2\text{T}_x$ paper can achieve a volumetric capacitance of 340 F/cm^3 at 2 mV/s , and nearly no loss is observed after 10,000 cycles at 1 A/g . This study has opened the door to the application and development of MXene in supercapacitors. Ghidiu et al. [6] initially used clay-like $\text{Ti}_3\text{C}_2\text{T}_x$ as a supercapacitor electrode and obtained a capacitance of 900 F/cm^3 (245 F/g) at 2 mV/s . The presence of smaller-sized H^+ improved the electrochemical performance compared to other intercalated cations. The accessibility of the interlayer spacing of the synthesized MXene after etching with LiF and HCl, as well as surface oxidation-reduction, also contributes to increased capacitance. To date, nearly 30 types of MXene have been successfully prepared, such as Ti_2C [91], V_2C [92], and V_4C_3 [93], and have shown promising potential as supercapacitor electrodes.

Research indicates that MXene holds promising potential in the field of supercapacitors. However, issues such as easy agglomeration and stacking of the material, as well as the surface functional groups' impact on the material's performance, have been identified. Researchers have attempted to modify MXene to achieve ideal performance, and composite materials are an important approach to improving energy storage performance by harnessing the advantages of combined materials. To obtain better performance, researchers have attempted to composite MXene with other types of materials, including polymers, metal hydroxides, metal oxides, and carbon materials [94–97].

4.1. Composite of MXene and Carbon Materials

Because of their special qualities, carbon materials, including graphene graphitylene and carbon nanotubes (CNTs), which are excellent conductors, make great composite possibilities for the energy storage industry [98,99]

CNTs are a typical one-dimensional carbon substance with wide application potential in the sphere of energy storage because of their distinctive morphology and prime electrochemical characteristics. They are incorporated into the electrodes of supercapacitors as active materials and carriers. Min Jae Ko et al. [100] uniformly electrodeposited a nickel-aluminum layered double hydroxide (Ni-Al-LDH) catalyst on MXene particles to ensure the uniform growth of multi-walled carbon nanotubes (MWCNTs). Subsequently, these catalytic MXene particles were likely altered using low-pressure chemical vapor deposition (CVD) at a temperature of $700 \text{ }^\circ\text{C}$ in argon flow. On the one hand, the grown MWCNTs act as spacers to prevent the MXene films from stacking again; on the other hand, they act as charge collectors within and between particles (Figure 4a,b). Additionally, their three-dimensional interconnected structure efficaciously enhances the stability of the combined electrode both mechanically and physicochemically. As shown in the CV curve in Figure 4c, due to the high charge transfer rate of MWCNTs and the high activity of MXene, 10-MWCNT-MXene@CC exhibits a larger CV curve area. An electrode prepared from this material demonstrated an excellent areal specific capacitance of $114.58 \text{ mF cm}^{-2}$ at a scan rate of 5 mV s^{-1} , as depicted in Figure 4d, along with an excellent cycling stability of 16,000 cycles (Figure 4e).

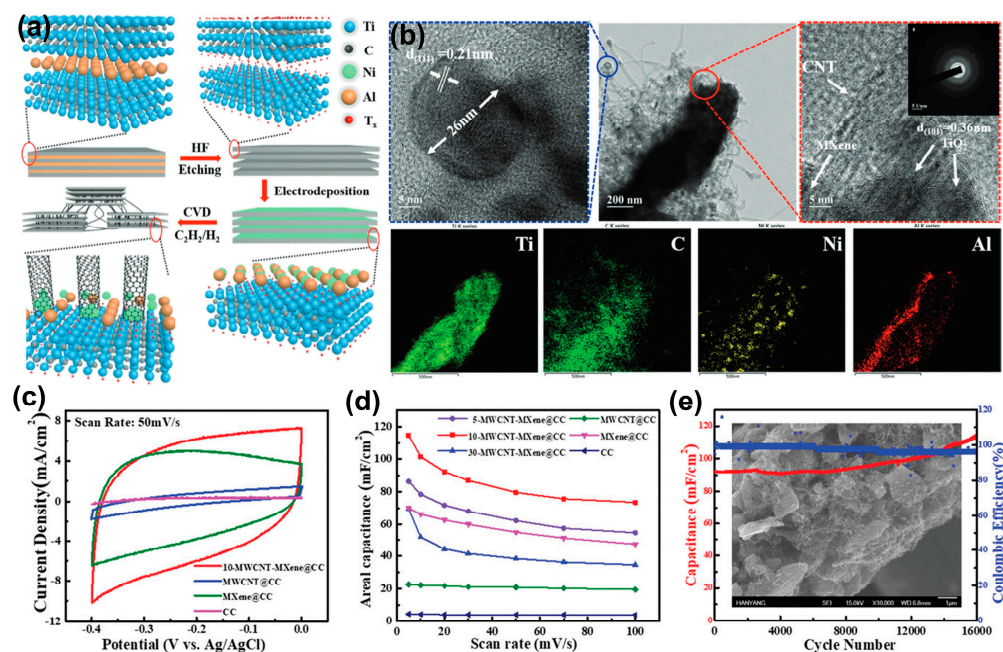


Figure 4. (a) Diagrammatic representation of the MXene and MWCNT preparation process. (b) TEM, high-resolution TEM images, and EDS maps of Ti, C, Ni, and Al of MWCNT-MXene composite. (c) Contrast of the current density across various electrodes at a 50 mV s^{-1} scan rate. (d) various samples' specific capacitance at various scan rates. (e) stability of cycling of 10-MWCNT-MXene@CC electrode on the condition of a current density of 10 mA cm^{-2} . Reproduced with permission [100]. Copyright 2020, John Wiley and Sons.

Graphene, a material with tremendous potential, has demonstrated its versatility in various fields. The composite research of graphene with other materials is also a hot spot that is usually studied regarding the storage of energy. MXene and graphene's combining together can efficaciously prevent graphene and MXene from stacking again, significantly increasing their particular area on the surface and particular capacity [101]. Liu et al. prepared a flexible and independent modified MXene/graphene oxide (MX-rHGO) thin film by filtering a mixture of MXene, which is alkalinized and porous graphene oxide (HGO) with mild tempering closely behind (Figure 5a) [99]. Implanted porous graphene efficaciously inhibits MXene's self-stacking, forming a nanoporous interconnected network that greatly accelerates ion transport and shortens the paths of both ions and electrons. If applied as an electrode material in supercapacitors, MX-rHGO₃ exhibits an ultrahigh volumetric capacitance (1445 F cm^{-3}) under a scan rate of 2 mV s^{-1} (Figure 5b) alongside an excellent rate performance and high mass loading. As a symmetric supercapacitor, MX-rHGO₃ retains 93% of its original capacity after 10,000 cycles at 5 A g^{-1} (Figure 5c). At a mass power density of 62.4 W Kg^{-1} , it achieves its greatest mass-energy density of 11.5 Wh Kg^{-1} (Figure 5d), and when its volume power density is 206 W L^{-1} , its volumetric energy density is 38.6 Wh L^{-1} (Figure 5e) [99]. An EIS curve can provide information about the ion transport in a composite, and a lower capacitance value usually indicates that the composite has a higher ion transport rate and better ion transport. When using composite materials, the interface formed by MXene or other materials can also affect the performance of capacitors, and the interface's impedance can affect the transmission efficiency of electrons and ions in the composite material. Therefore, the impact of the interface on the material can be evaluated through an analysis of its impedance characteristics. For example, an MX-rHGO₃ electrode material has a lower coactance, which can further improve the performance of low-voltage capacitors. To further elucidate the ion transport kinetics of MXrHGO, MX-rGO, and pure MXene membranes, electrochemical impedance spectroscopy (EIS) measurements have been performed, with frequencies ranging from 0.01 HZ to 100 KHz. The curve shows that the interfacial charge transfer resistance (Rct) of MX-rHGO₃ is significantly lower than that of the pure MXene membrane and MX-

rGO₃ membrane, which means that the ionic conductivity of the MX-rHGO₃ membrane improved after the embedding of porous graphene and subsequent annealing treatment. In addition, the MX-rHGO₃ membrane also has low diffusion resistance, mainly because the embedded porous graphene provides more active sites, and the removal of surface groups after the annealing treatment further promotes ion transport. It can be seen that the changes in impedance characteristics reflect the degree to which the material obstructs electron transport, while a lower resistance indicates that the composite material has a better electron transport performance and that electrons can be easily conducted in that material.

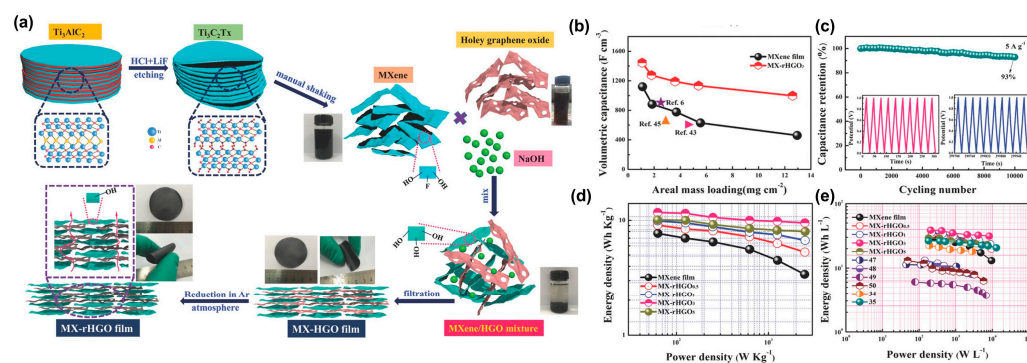


Figure 5. (a) demonstration of a combination of the qualified MXene/holey graphene film. (b) The outcome of areal mass loading on the volumetric capacitance of MXene film and MX-rHGO₃ compared to several former reports. (c) Capacitance retention of MX-rHGO₃-based symmetric supercapacitor on the condition of a density of electricity of 5 A g⁻¹ for 10,000 cycles, unchanging electricity charge-discharge curve graphs of the original ten cycles and last ten cycles are displayed in the inset. (d) Gravimetric and (e) MX-rHGO₃-based symmetric supercapacitors' volumetric energy and watt densities compared to former reports. Reproduced with permission [99]. Copyright 2018, John Wiley and Sons.

Due to MXene's unique sp and sp² carbon hybrid orbitals, the adjustability of its electronic structure and pore structure is enhanced. Because of this characteristic, it provides an ideal platform for the mechanism research and performance optimization of supercapacitors [98]. The performance of capacitors can be greatly affected by varying their stacking modes. For example, wang et al. constructed an independent, flexible, three-dimensional (3D), interconnected, and hydrated ion-permeable MXene/graphitic diyne nanotube (MG) composite film [96]. This composite material has excellent capacitor performance, and the three-dimensional embedding effect of GDY-NTs can solve the problem of MXene's heavy stacking, shorten the ion transport path, and reduce ion transport resistance. In addition, the synergistic effect of horizontal and vertical three-dimensional intercalation and the abundant in-plane holes in GDY-NTs are also the key reasons for the improved capacitance and magnification performance of MG films. This work provides a reference for solving the re-stacking problem of MXene.

4.2. Composite of MXene and Metal Oxides Materials

Transition metal oxides (TMOs) possess characteristics like high theoretical volume, being economical, as well as unique mechanical and electrochemical properties. However, they suffer from severe volume expansion between charge and discharge, inadequate charge transfer capability, and low conductivity, resulting in poor rate performance and cycling stability. By combining TMOs with conductive materials such as MXene, their respective advantages can be exploited to improve material performance [95,102].

Among all TMOs, the combination research of manganese dioxide (MnO₂) with MXene is the most extensive. On the one hand, MnO₂ has a high theoretical capacitance of 1370 F g⁻¹, and its electrochemical window is as wide as 0–0.9 V; on the other hand, it can also operate in mild aqueous electrolytes with minimal chemical corrosion to current collectors [103,104]. Although the low electronic conductivity and dissolution of Mn in the redox reactions lead to lower capacitance and shorter cycle life of MnO₂-based materials, the combination of

MnO₂ with MXene can achieve excellent performance supercapacitor properties. For example, Luo et al. [105] grew MnO₂ nanoflowers on exfoliated ultrathin Ti₃C₂T_x MXene nanosheets using a co-precipitation method (Figure 6a), forming MNF/Ti₃C₂T_x. This material features a two-dimensional sheet structure with a large surface area, the advantages of porous MnO₂ nanoflowers, and a highly conductive electronic structure. The optimized MNF/Ti₃C₂T_x electrode exhibits an excellent electrochemical capacitance performance. The galvanostatic charge-discharge (GCD) curve in Figure 6b shows that the best-performing MNF (80%)/Ti₃C₂T_x sample achieves a capacitance of 348.5 F g⁻¹ at an electricity density of 0.5 A g⁻¹, which is 2.3 and 2.6 times higher than that of MnO₂ and Ti₃C₂T_x. MNF (80%)/Ti₃C₂T_x's performance remains at 67% when the electricity density rises from 0.5 A g⁻¹ to 8 A g⁻¹, showing an excellent rate capability. AC impedance results demonstrate the material's enhanced electron transport, effectively accelerating its electrochemical kinetics. The cycling stability test results in Figure 6f,g show that MNF (80%)/Ti₃C₂T_x's performance retention rate reaches 91.9% after 5000 cycles, which is significantly higher than that of MnO₂ (68.3%) and Ti₃C₂T_x (59.2%). The extended durability of MNF (80%)/Ti₃C₂T_x can be attributed to its MnO₂ nanoflowers interacting intensely with its Ti₃C₂T_x matrix.

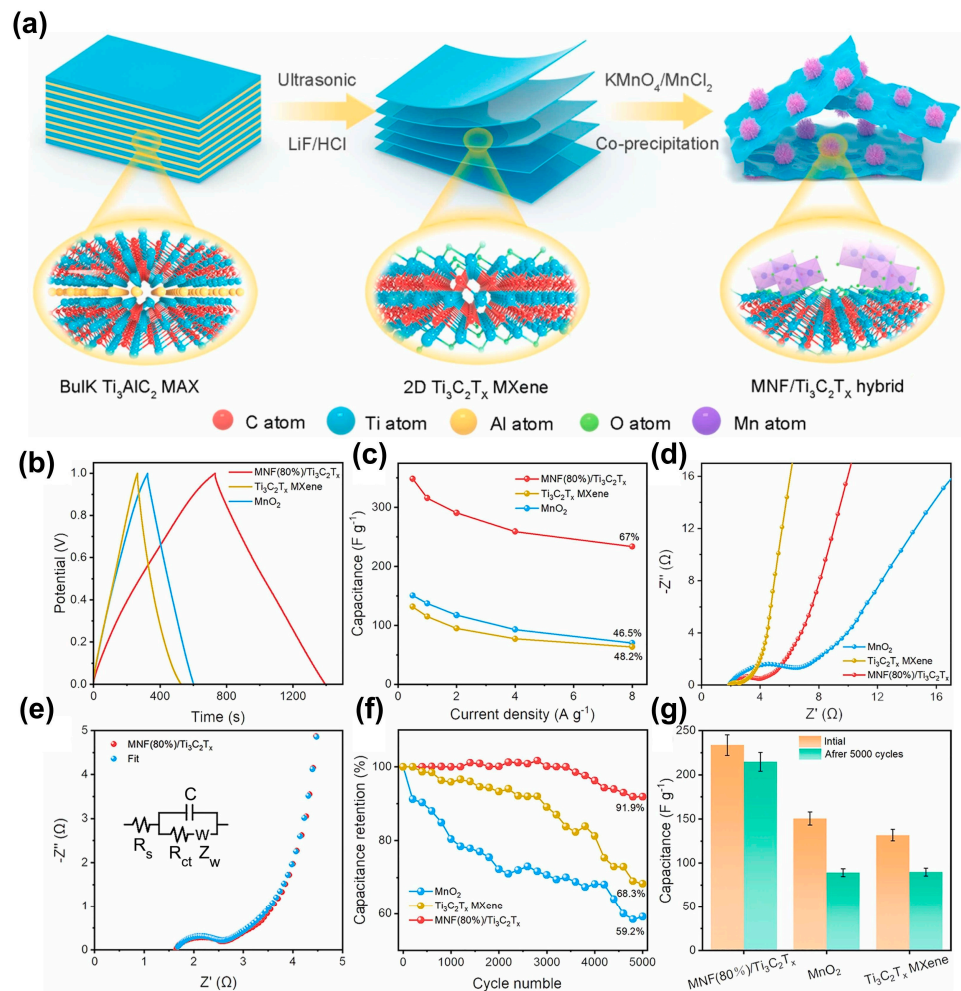


Figure 6. (a) Diagrammatic representation for the combination of the MNF/Ti₃C₂T_x nanoarchitectures. (b) GCD curve graphs of the MNF(80%)/Ti₃C₂T_x, MnO₂, and Ti₃C₂T_x electrodes with an electricity density at 0.5 A g⁻¹. (c) Difference of the specific capacitance when electricity density is MNF(80%)/Ti₃C₂T_x, MnO₂, and Ti₃C₂T_x electrodes. (d) AC impedance spectra of the MNF(80%)/Ti₃C₂T_x, MnO₂, and Ti₃C₂T_x electrodes and (e) the consistent fitting curve. (f,g) Cycling stability of the MNF(80%)/Ti₃C₂T_x, MnO₂ and Ti₃C₂T_x electrodes. Reproduced with permission [105]. Copyright 2023, Elsevier.

EIS is a technique concerned with detecting the electrical resistance and electron transfer properties of an electrode material. The AC impedance spectrum provides information about the internal resistance of the electrode and the resistance between the electrolyte and the electrode. Some researchers have also studied MXenes' impedance characteristic curves, describing the Nyquist diagrams of the EIS spectra of MnF, MXene, and their complexes, with a frequency range of 100 KHz to 0.1 Hz [95]. The slant period in the high-frequency region of a Nyquist curve is coupled with the slant line in its low-frequency region such that the charge transfer resistance can be calculated. The Rct of MnF/MXene nanocomposites is the smallest, which is believed to be due to the dispersion of MnF nanoparticles across MXene nanosheets and the existence of MNF nanoparticles between multilayer MXene sheets to promote the flow of electrons. In comparison with RuO₂, its composite exhibits very stable behavior, with slight changes in current density during its first few hours of use due to the activation of the manufactured substance and the opening of the electrode's active site. Therefore, we believe that a composite of MXene and a metal oxide is an effective method of promoting a material's properties.

In addition to manganese oxide, nickel, cobalt, iron-based oxides are also of interest due to their low cost, electrochemical capacitance behavior, environmental friendliness, and high theoretical capacitance [106]. However, there is still limitation on their ability of cycling and power density due to the poor electronic conductivity kinetics. More strategies need to be improved, such as establishing distinctive layered structures or adding heterogeneous materials like 2D MXene materials.

Figure 7a illustrates the synthesis of hybrid, porous Co₃O₄-MXene/RGO aerogels. The 2D MXene material is obtained by etching Ti₃AlC₂ using HF, and Co₃O₄ nanoparticles are grown on its surface to form Co₃O₄-MXene. The Co₃O₄-MXene is then combined with GO, freeze-dried, and thermally reduced to obtain hybrid, porous Co₃O₄-MXene/RGO aerogels. This material performs outstandingly in the field of electrochemistry. The GCD curve in Figure 7b demonstrates that its specific capacitance is very high, reaching 345 F g⁻¹ at an electricity density of 1 A/g. After 10,000 charge-discharge cycles, it retains 85% of its original specific capacitance, indicating its good cycling stability (Figure 7c) [107]. In addition to single-metal oxides, there has also been extensive research on multi-metal oxides. Wang et al. prepared a 2D NiMoO₄ nanosheet-MXene composite (NiMoO₄/M₁₀) using a combination of hydrothermal and thermal treatment methods (Figure 7d). Their GCD and specific capacity results (Figure 7e,f) showed that, at a current density of 1 A/g, the specific capacitance of the NiMoO₄/M₁₀ electrode is 483.8 C g⁻¹, surpassing that of the NiMoO₄ electrode (332.7 C g⁻¹). Moreover, its capacitance decay is insignificant in the range of 1 to 20 A g⁻¹ [108]. Xie et al. fabricated a composite film through the filtration of MXene nanosheets and Co-Fe oxide (Figure 7g). Electrochemical performance tests (Figure 7h,i) demonstrated that the composite film with an 8% Co-Fe oxide/Ti₃C₂T_x ratio exhibited the best performance, with a specific areal capacitance of 1236.3 mF cm⁻² at a current density of 0.2 mA cm⁻² [109]. These research findings indicate that the addition of Ti₃C₂T_x to oxide electrode materials leads to their higher specific capacitance and greater performance stability at high rates, making oxides promising for supercapacitor applications.

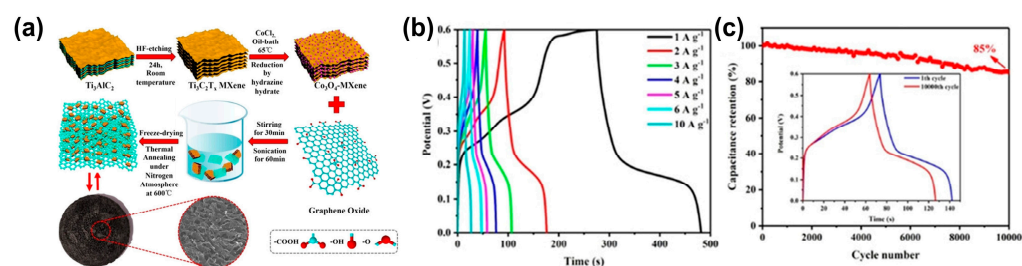


Figure 7. Cont.

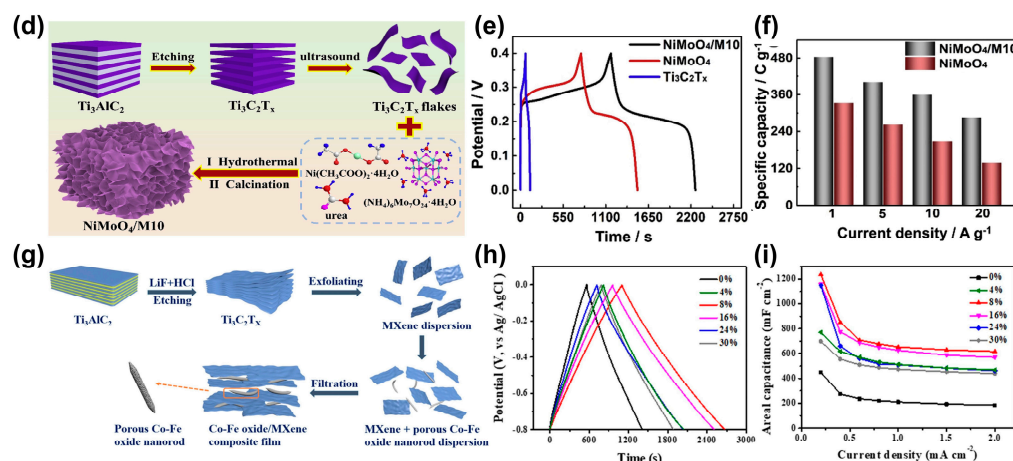


Figure 7. (a) Diagrammatic representation of preparing the Co_3O_4 -MXene/RGO hybrid porous aerogels step by step. (b) GCD curves of Co_3O_4 -MXene/RGO (Co_3O_4 -MXene/GO mass ratios of 3:1) electrode at various electricity densities ranging from 1 to 10 Ag^{-1} . (c) The stability of cycling of the Co_3O_4 -MXene/RGO electrode during 10,000 cycles at an electricity density of 3 Ag^{-1} is demonstrated by the inset that curves of CV obtained at the 1st and 10,000th cycles. Reproduced with permission [107]. Copyright 2019, John Wiley and Sons. (d) Diagrammatic representation for the NiMoO_4 /M10 hybrids' combination process. (e) Contrasting GCD plots of NiMoO_4 /M10, NiMoO_4 , and $\text{Ti}_3\text{C}_2\text{T}_x$ electrodes at an electricity density of 0.5 A g^{-1} . (f) Contrast between the capacities of NiMoO_4 /M10 and NiMoO_4 electrodes at various electricity densities. Reproduced with permission [108]. Copyright 2019, Elsevier. (g) Diagrammatic representation of the combination of Co-Fe oxide/MXene composite membrane. (h) GCD curves of MXene and Co-Fe oxide/ $\text{Ti}_3\text{C}_2\text{T}_x$ membranes range among ratios of various masses, with the electricity density being 0.4 mA cm^{-2} . (i) Particular areal capacitance of different samples versus current density. Reproduced with permission [109]. Copyright 2020, Elsevier.

4.3. Composite of MXene and Metal Hydroxide Materials

Layered metal hydroxides have a large amount of positive charge, significant theoretical capacity, a relatively large specific surface area, and adjustable composition. However, they exhibit poor intrinsic conductivity and significant aggregation tendencies, the results of which are inferior performance of rate and stability of cycling. The synergistic effect of different materials significantly increases the exposed active sites in redox reactions, enhancing the electrode's activity. Composite electrodes generate many electrochemically active centers, improve electrical conductivity, and exhibit superior pseudocapacitive storage performance. Therefore, the combination of metal hydroxides with MXene effectively improves the aggregation of metal hydroxides, alleviates the self-stacking effect of MXene, as well as enhancing the performance of the electrode electrochemically [96,110]. Liang et al. prepared a flower-shaped hollow NiMnCoOH@MXene composite material by electrostatically adsorbing a colloidal solution onto a few-layer or single-layer etched $\text{Ti}_3\text{C}_2\text{T}_x$ MXene and a NiMn-MOF precursor and then subjecting the composite to hydrothermal treatment in the presence of Co ions (Figure 8a) [111]. SEM images show that the nano-flower-shaped NiMnCoOH@MXene composite material is a hollow nanosphere with an average diameter of $2.2 \mu\text{m}$, covered with many extremely thin MXene sheets (Figure 8b,c), in which larger MXene nanosheets play the role of bridges, connecting and promoting the building of a three-dimensional network of conductivity. The porous morphology of the composite material provides a surface area that is highly specific, and the nano-flower-shaped structure further enhances its structural stability and mechanical strength. This hierarchical, hollow, flower-like construction provides abundant active sites and channels for transporting ions, facilitating ion transport and charge storage and contributing to its outstanding electrochemical performance. The GCD curve in Figure 8d indicates that the charge-discharge time of the NiMnCoOH@MXene composite material electrode is longer

than that of the NiMnCoOH electrode. At a current density of 1 A g^{-1} , the specific capacitance of the NiMnCoOH@MXene composite material and NiMnCoOH are $232.37 \text{ mAh g}^{-1}$ (1521 F g^{-1}) and $154.76 \text{ mAh g}^{-1}$ (1013 F g^{-1}), demonstrating the positive effect of MXene's introduction on capacitance performance. Figure 8e shows that, at current densities of 1, 2, 5, and 10 A g^{-1} , the specific capacitance of the NiMnCoOH@MXene composite material is calculated to be 232.37, 223.36, 192.95, and $154.61 \text{ mAh g}^{-1}$. When moving from 1 to 10 A g^{-1} , the specific capacity retention rate of the NiMnCoOH@MXene composite material reached 66.22%, while that of NiMnCoOH was only 54.32%. This is due to the enhanced conductivity of the NiMnCoOH@MXene composite material (Figure 8f). The data above indicate that the electrochemical performance, specific capacity, and conductivity of nano-flower-like, hollow NiMnCo-OH modified by self-assembled 2D $\text{Ti}_3\text{C}_2\text{T}_x$ can be significantly improved. MXene suppresses the morphological breakdown of metal hydroxides and significantly improves their specific capacity, while the conductivity of MXene increases the number of available electrons on hydroxides. A composite structure composed of MXene and a metal hydroxide also impacts the impedance characteristics of the electrode material. For example, the impedance of the NiFe-LDH/MXene composite is reduced with the addition of MXene [110]. The Nyquist plots for NiFeLDH, MXene, and NiFeLDH/MXene (60 mg) are all composed of arcs in their high-frequency regions and linear shapes in their low-frequency regions. The curve seen at high frequencies is interpreted as the internal resistance of the active material, the ionic resistance of the electrolyte, and the contact resistance in the electrode. The results show that the internal resistance of the NiFe-LDH/MXene composite is lower than that of pure LDH, which indicates that the addition of MXene provides more conductive transmission paths for electron transport and effectively improves the conductivity of the material.

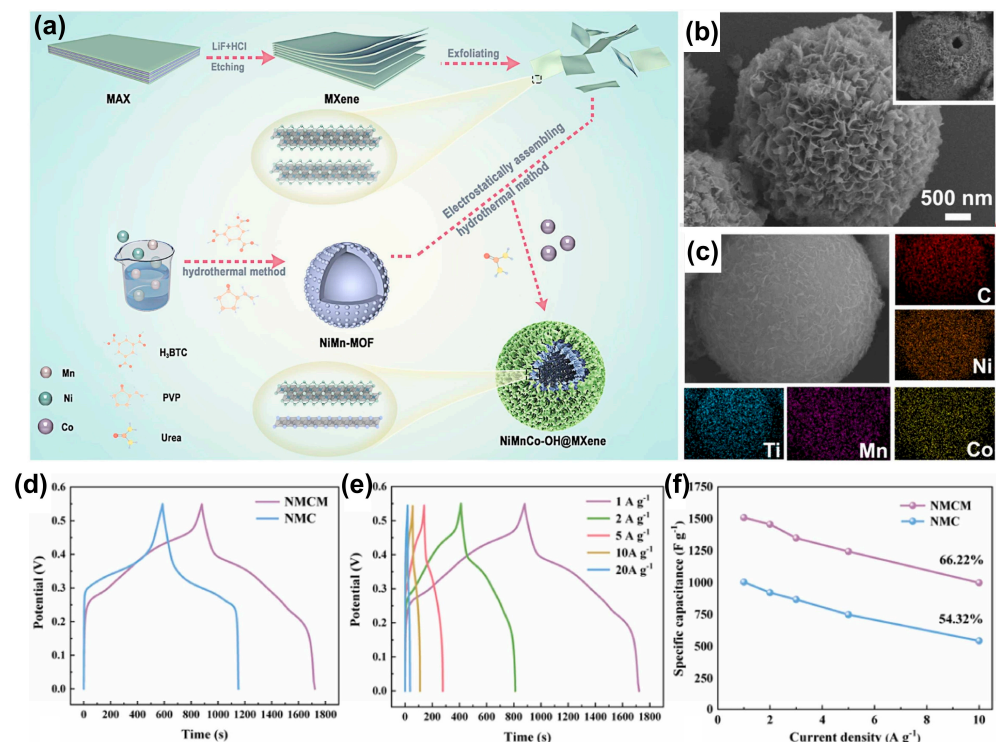


Figure 8. (a) Composite diagram of NMCM hollow spheres. (b) SEM graphs of NiMnCoOH@MXene (it is at the left corner on the top that the hollow structure of NiMnCoOH@MXene is demonstrated). (c) EDS elemental mapping of C, O, Ni, Co, Mn, and Ti in NiMnCoOH@MXene. (d) GCD diagrams for NiMnCoOH and NiMnCoOH@MXene (under optimum conditions) tested at 1 A g^{-1} . (e) GCD diagrams of NiMnCoOH@MXene under various current densities. (f) Capacitance values in different current densities of NiMnCoOH and NiMnCoOH@MXene. Reproduced with permission [111]. Copyright 2024, Elsevier.

4.4. Composite of MXene and Conductive Polymer Materials

MXene and conductive polymers are both research hotspots in the field of supercapacitor electrode materials. Combining these two distinctive types of materials together, the shortcomings can be addressed if it is applied individually as electrode materials. Based on theoretical capacity, specific surface area, mass loading, flexibility, and outstanding mechanical properties, MXene/conductive polymer composite materials have great prospects of becoming higher-level electrode materials. Introducing polymers can efficaciously increase the space between each layer of MXene, providing support, inhibiting stacking of MXene layers, facilitating the exposure of more active surface sites, shortening the path on which the electrolyte ions may diffuse, promoting the transport of electron and rapid Faradaic reactions, and improving mechanical performance and material stability. In a study by Wang et al., highly conductive polyaniline nanoparticles (PANI NPs, ~ 10 nm) were used as embedments to regulate the intercalation of MXene nanosheets via a self-assembly method [112]. The interlayer PANI NPs not only inhibit the self-stacking of MXene but also make more ion transport routes possible. In addition, Wu et al. deposited accordion-like N-Ti₃C₂/PANI composite materials on FTO glass surfaces via electrochemical reactions [113]. During the reaction process, amino-functionalized N-Ti₃C₂ sites combined with the amine nitrogens in the PANI chains, promoting the development of aniline between the Ti₃C₂ layers (Figure 9a). The strengths of accordion-like Ti₃C₂ MXenes/PANI materials include effectively preventing N-Ti₃C₂ from stacking densely during its electrochemical polymerization, facilitating electron transport, and providing numerous active sites for high-speed charge carrier transport. N-Ti₃C₂ is an excellent matrix for conductivity (Figure 9b), and the combination of N-Ti₃C₂ with polyaniline effectively utilizes various mechanisms to store energy to enhance the electrochemical effect of supercapacitors. The GCD curve in Figure 9c shows nearly triangular shapes when the current density is 0.5 mA cm⁻², suggesting that the capacitors' behavior is ideal and reversible. The N-Ti₃C₂/PANI-420 electrode has the longest discharge time and the highest specific capacitance. Figure 9d demonstrates that as the testing current density increases, the capacitance decreases. The specific capacitance of N-Ti₃C₂/PANI-420 is 117.10 mF cm⁻² at a current density of 0.5 mA cm⁻², surpassing that of other electrodes and notably outperforming the N-Ti₃C₂ electrode. These results indicate that the synthesis of two different materials can enhance the electrochemical performance of N-Ti₃C₂/PANI composite materials, with PANI chains helping to prevent the dense stacking of Ti₃C₂ MXenes, facilitating the diffusing of ions and providing greater electrochemical activity. As a conductive additive, MXene can provide high conductivity and a large surface area, and its combination with conductive polymers can increase the effective electrode surface area of capacitors, thereby increasing their capacity. This means that these composite materials can store more charge, increasing the energy density of capacitors. Furthermore, the high conductivity of MXene, combined with the conductivity of a conductive polymer, can speed up the transfer rate of charge in the capacitor. This means that capacitors can be charged and discharged faster and with a higher power density. Ti₃C₂ MXenes/PANI materials, for example, can effectively prevent the dense accumulation of N-Ti₃C₂ during electrochemical polymerization, promote electron transport, and provide numerous active sites for high-speed charge carrier transport. Moreover, Pathak et al. prepared MXenes containing hollow carbon nanofibers (MXHCNFs) via co-axial electrospinning; the inside surface of the MXHCNFs is decorated with polypyrrole layers (PPy@MXHCNF) [114], which are sufficiently flexible, conductive, and highly functionalized, and have a unique trilayer morphology. This work takes a unique approach that involves modifying MXenes to create polypyrrole-decorated electrospun MXHCNFs, which are efficient substrates for freestanding electrodes, as a common strategic route for creating both positive and negative electrodes for flexible asymmetric supercapacitors.

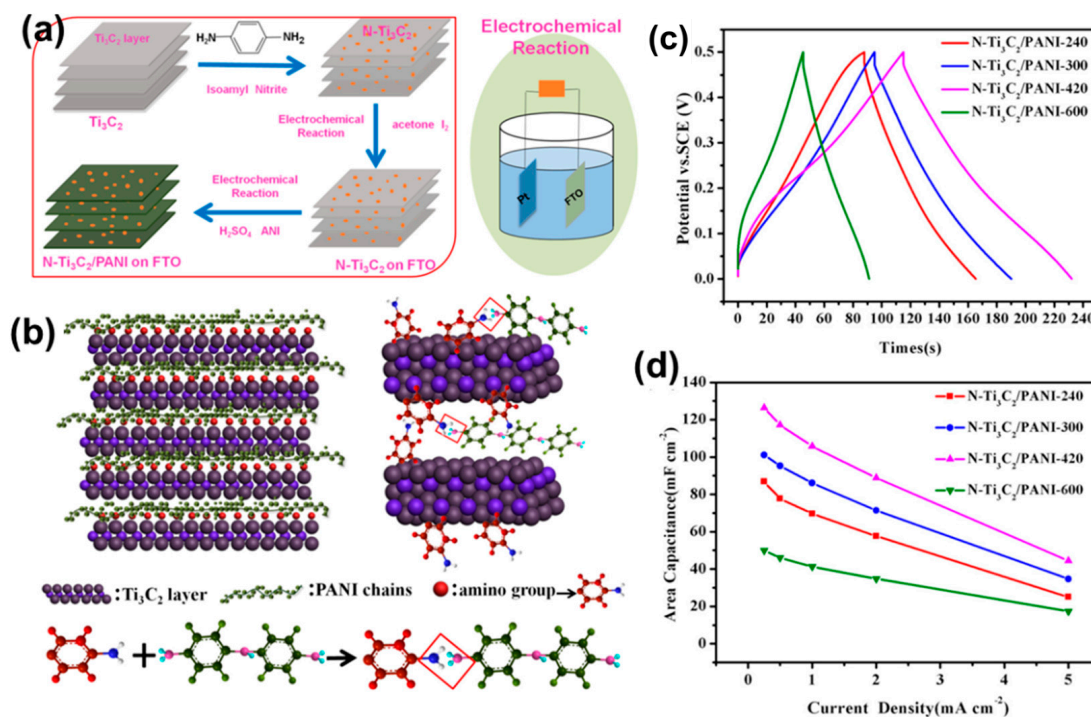


Figure 9. (a) Diagrammatic representation for the fabrication of N-Ti₃C₂/PANI. (b) Atomic schematic of intercalated PANI in the interlayers of N-Ti₃C₂. (c) Representative GCD curves on the condition of the current density being 0.5 mA cm⁻². (d) Specific capacitance on the condition of various current densities from 0.25 to 5 mA cm⁻². Reproduced with permission [114]. Copyright 2019, Elsevier.

4.5. Composites of MXene and 2D Materials

MXene materials have also been widely applied in capacitors through their combination with other 2D materials such as MoS₂ [115] and MoSe₂ [116,117]. Compared to traditional batteries, capacitors have a lower energy density, so improving their electrode materials is particularly important for enhancing their energy storage capacity. MXene materials have good conductivity and morphological characteristics, while MoS₂ is a graphite-like material with a high ion conductivity and energy storage capacity. Combining these two materials allows for energy storage across a larger voltage range and an overall increase in capacitance. For instance, in their preparation of MoS₂/MXene materials (Figure 10a), Chandran et al. improved MXene by etching it [118]. Through multiple characterizations, they discovered that this material exhibited a maximum specific capacitance of up to 342 F g⁻¹ across an extended voltage range (Figure 10b). However, the van der Waals forces between MXene layers can lead to their stacking and aggregation, causing a loss of electrochemically active sites. This issue can be addressed by using other 2D materials to enhance the construction of MXene-based electrodes, thereby producing supercapacitors with excellent electrochemical performance [115]. For example, Chen et al. introduced layered MoSe₂ nanosheets into MXene (Figure 10c), creating a unique heterostructure with an enhanced active region for redox reactions that also exhibits good synergistic effects [119]. This composite material demonstrated a higher specific capacitance of 1358.5 F g⁻¹ (Figure 10d), not only improving the energy density of the capacitor but also maintaining its high-power density and long cycling life. It is a promising candidate material for supercapacitors. In summary, research on the combination of MXene materials with other 2D materials provides a broader material design approach for developing supercapacitors with high-energy density and superior electrochemical performances [120]. It also offers an important scientific foundation for achieving sustainable energy conversion and storage.

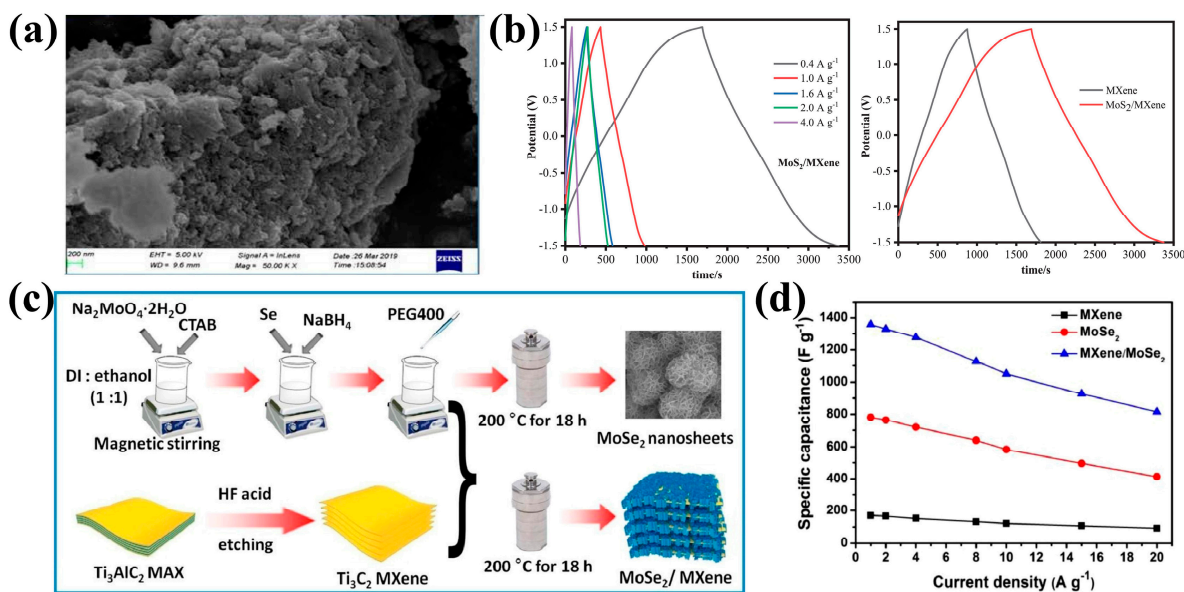


Figure 10. (a) SEM images of MoS₂/MXene (b). Galvanostatic charge-discharge curve of MoS₂/MXene at current density 0.4, 1, 1.6, 2, and 4 A g⁻¹. and MXene and MoS₂/MXene at 0.4 A g⁻¹ [118]. Copyright 2020, Elsevier. (c) Schematic of the growth procedures of Ti₃C₂T_x MXene/MoSe₂ hybrid composites. (d) specific capacity of MXene, MoSe₂, and MXene/MoSe₂ [119]. Copyright 2021, Elsevier.

MXene is a two-dimensional material consisting of a multilayer, sheet-like structure of transition metal carbides or nitrides. It has excellent electrical conductivity and chemical stability, and thus, it has attracted much attention in the field of electronic devices and energy storage. In summary, it can be concluded that composites of MXene and other materials are the reason for the improvement in the performance of composite supercapacitors (Tables 2 and 3). Changes in the impedance characteristic curves of MXene and polymer composites might have the following effects on the performance of capacitors:

1. Reduce electrolyte resistance: MXene has a high conductivity and can effectively reduce the resistance of the electrolyte when it is combined with polymers. This will reduce the resistance loss inside the capacitor and improve the efficiency of its energy transfer.
2. Improve the frequency response of the capacitor: After MXene is combined with a polymer, the surface area of the capacitor may be increased, and its effective capacitance may be improved. At the same time, in the high-frequency band, the impedance characteristic curve of the composite material may be closer to the ideal behavior of the capacitor so that the capacitor has a better performance in high-frequency applications.
3. Improve the cycle stability of capacitors: MXene's high chemical stability can improve the cycle life and stability of capacitors. A change in the impedance curve of a composite material may manifest as a smaller phase angle drift and a more stable electrochemical interface, which reduces the performance attenuation of the capacitor over a long cycle of charge and discharge.
4. Adjust the charge and energy storage behavior of the capacitor: Changes in the impedance characteristic curves of MXene and polymer composites may lead to changes in the charge storage mechanism and energy storage behavior of capacitors. This may include adjustments in capacitors' capacity, voltage response, charge/ion transfer rate, etc., that improve their performance.

Table 2. Performance of recent other MXene-based composite materials.

Mxene	Capacitance Value	Energy Density	Power Density	Stability	Ref.
Mxene/ZnCl ₂ //MnO ₂ -MWCNTs	529.1 F g ⁻¹ , 1.00 mV s ⁻¹	90.1 Wh kg ⁻¹	185.0 W kg ⁻¹	capacity retention rate of 86.9% after 12,000 cycles	[121]
HS-NCS@MXene//AC-AHSC	2637 F g ⁻¹ , 2.5 A g ⁻¹	80 Wh kg ⁻¹	1196 W kg ⁻¹	stable cycling life (96%) over 10,000 cycles	[122]
MXene/AuNPs	278 F·g ⁻¹ , 5 mV·s ⁻¹	8.82 Wh·L ⁻¹	264.6 W·L ⁻¹	reaches 95.0% after 10,000 cycles.	[123]
MXene/PZS//AC	380 F g ⁻¹ , 2 mV s ⁻¹	12.26 Wh kg ⁻¹	125.00 W kg ⁻¹	remarkable cycling stability without obvious deterioration after 5000 cycles	[124]
MIL-100(Fe)/Ti ₃ C ₂	962.17 F g ⁻¹ , 0.5 A g ⁻¹	85.53 Wh kg ⁻¹	200 W kg ⁻¹	The capacity retention rate was 93% up to 10,000 cycles at 5 A/g	[125]
Ti ₃ C ₂ T _x -Mn	248 F g ⁻¹ , 100 A g ⁻¹	38.40 Wh kg ⁻¹	55.30 Wh kg ⁻¹	an excellent cycle life with 85.53% retention after 100,000 cycles at a current density of 100 A g ⁻¹	[126]

Table 3. Performance of recent MXene-based composite materials.

Devices	Electrolyte	Capacitance	Energy Density at Power Density	Ref.
MXene//PANI@MXene	3 M H ₂ SO ₄	87 Fg ⁻¹ , 10 mVs ⁻¹	50.6 WhL ⁻¹ at 1.7 kWL ⁻¹ 24.4 WhL ⁻¹ at 127 kWL ⁻¹	[127]
GMP//graphene	1 M H ₂ SO ₄	68 Fg ⁻¹ , 10Ag ⁻¹	42.3Whkg ⁻¹ at 950 Wkg ⁻¹ 25 Whkg ⁻¹ at 18,000 Wkg ⁻¹	[128]
Ti ₃ C ₂ T _x /Fe-15%//MnO ₂ /CC	1 M Li ₂ SO ₄	115 mF cm ⁻² , 2 mA cm ⁻²	40mWh cm ⁻² at 8.2 mW cm ⁻²	[129]
Ni-dMXNC//Ti ₃ C ₃ T _x	1 M KOH	-	1.04×10 ⁻³ Wh cm ⁻³ at 0.22 W cm ⁻³	[130]
MXene//PANI/MXene	1 M H ₂ SO ₄	231 F cm ⁻³ , 10 mV s ⁻¹	65.6 Wh L ⁻¹ at 1687.3 W L ¹	[131]
Ti ₃ C ₂ T _x /P-100-H//rGO	1 M H ₂ SO ₄	117 F cm ⁻³ , 1.5 mA cm ⁻²	23 mWh cm ⁻³ at 7659 mW cm ⁻³	[132]
MXene/PPy//MXene/PPy	1 M H ₂ SO ₄	184 F g ⁻¹ , 10 mV s ⁻¹	-	[133]
400PPy175/Ti ₃ C ₂ T _x //400PPy175/Ti ₃ C ₂ T _x	1 M H ₂ SO ₄	258 F g ⁻¹ , 0.5 A g ⁻¹	10.82 μWh mg ⁻¹ at 0.11 mW mg ⁻¹	[134]
AC//MXene/PANI	7 M KOH	262 F g ⁻¹ , 0.5 A g ⁻¹	22.67 Wh kg ⁻¹ at 217 W kg ⁻¹	[135]
Mo _{1.33} C MXene/PEDOT:PSS//Mo _{1.33} C MXene/PEDOT:PSS	1 M H ₂ SO ₄	568 F g ⁻¹ , 0.5 A g ⁻¹	33.3 mWh cm ⁻³ at 19,470 mW cm ⁻³	[136]
Ti ₃ C ₂ T _x //Ti ₃ C ₂ T _x	Sea water	27 F cm ⁻³ , 0.25 A g ⁻¹	1.74 × 10 ⁻³ Wh cm ⁻³ at 0.15 W cm ⁻³	[137]
Ti ₂ CT _x //Ti ₂ CT _x	1 M KOH	452 F cm ⁻³ , 2 mV s ⁻¹	35 mWh cm ⁻³ at 0.49 W cm ⁻³	[138]
M-NC@NCM/NF//AC	--	118.5 F·g ⁻¹	32.6 Wh·L ⁻¹ /699.6 W kg ⁻¹	[139]
MnO ₂ @MXene/CNT	1mol·L ⁻¹ H ₂ SO ₄	371.1F·cm ⁻³ @1 A·cm ⁻³	8.22 mWh·cm ⁻³ /276.28 mW·cm ⁻³	[140]

Table 3. Cont.

Devices	Electrolyte	Capacitance	Energy Density at Power Density	Ref.
MnO ₂ /Ti ₃ C ₂ T _x	1mol·L ⁻¹ Na ₂ SO ₄	130.5F·g ⁻¹ @0.2 A·g ⁻¹	-	[141]
Co ₃ O ₄ -Nb ₂ C	6mol·L ⁻¹ KOH	1061 F·g ⁻¹ @2 A·g ⁻¹	60.3 Wh·kg ⁻¹ /670 W·kg ⁻¹	[142]
Co-MXene	6mol·L ⁻¹ KOH	1081F·g ⁻¹ @0.5 A·g ⁻¹	26.06 Wh·kg ⁻¹ /700 W·kg ⁻¹	[143]
MoO ₃ NWs/MXene@CC	2mol·L ⁻¹ KOH	775 F·g ⁻¹ @1 A·g ⁻¹	-	[144]
Ti ₃ C ₂ T _x /CoS ₂	2mol·L ⁻¹ KOH	1320 F·g ⁻¹ @1 A·g ⁻¹	-	[145]
NiCo ₂ Se ₄ /MXene	3mol·L ⁻¹ KOH	953.8 F·g ⁻¹ @1 A·g ⁻¹	22.4 Wh·kg ⁻¹ /800 W·kg ⁻¹	[146]
Ti ₃ C ₂ T _x /Ni-MOFs	6mol·L ⁻¹ KOH	1124 F·g ⁻¹ @1 A·g ⁻¹	24 Wh·kg ⁻¹ /8 kW·kg ⁻¹	[147]
MP/FM/MP-20%	1 M H ₂ SO ₄	388 F·g ⁻¹	17.45 Wh kg ⁻¹	[148]
MX/PANI NPs	--	377 F g ⁻¹	90.3 μWh cm ⁻²	[112]
Ti ₃ C ₂ T _x /CMC-PANI (TCP) film	1 M H ₂ SO ₄	1161.4 mF cm ⁻² @1 mA cm ⁻²	158.7 μW h cm ⁻² at 700.1 μW cm ⁻²	[149]
TDP	1 M H ₂ SO ₄	452 F g ⁻¹ @1 A g ⁻¹	-	[150]

It is important to note that specific effects depend on the ratio of MXene to polymer, the preparation method used, and the specific design and application requirements of the capacitor. These factors will affect the impedance characteristic curve of the composite material and the performance of the capacitor. Therefore, in specific applications, experimental studies and performance evaluations are required to determine the composite's optimal composition and design parameters.

5. Influence of Electrolytes on the Performance of MXene-Based Supercapacitors

Electrolytes play a crucial role in the assembly of supercapacitors as they directly affect the ion transport efficiency and stable potential window of the electrochemical system. In general, Ti₃C₂T_x exhibits a higher capacitance in aqueous solutions, especially in H₂SO₄, and possesses a wider operating voltage range in organic electrolytes.

5.1. Alkaline Electrolytes

Lukatskaya et al. successfully fabricated a flexible, hydrophilic, binder-free, and additive-free Ti₃C₂T_x as an electrode for supercapacitors [90]. This Ti₃C₂T_x was utilized in a potassium hydroxide (KOH) electrolyte, resulting in a remarkable volumetric capacitance of 340 F cm⁻³ (Figure 11a). This capacitance surpasses that of activated microwave-expanded graphite oxide (60–100 F cm⁻³) and carbide-derived carbons (180 F cm⁻³) [151]. Their electrochemical system, comprising the Ti₃C₂T_x as the working electrode, KOH as the electrolyte, Ag/AgCl as the reference electrode, and activated carbon (AC) as the counter electrode, exhibited a potential window of 0.55 V. Furthermore, the capacitance achieved using KOH as the electrolyte (approximately 130 F g⁻¹) surpassed those obtained when using sodium acetate (NaO Ac) (approximately 120 F g⁻¹) and magnesium sulfate (MgSO₄) (approximately 100 F g⁻¹) as the electrolytes (Figure 11b). Gao et al. also reported on a symmetric supercapacitor employing a Ti₃C₂T_x electrode with a binder and carbon black in a KOH electrolyte, which exhibited a capacitance of 71.2 F g⁻¹ and a potential window of 0.9 V [152].

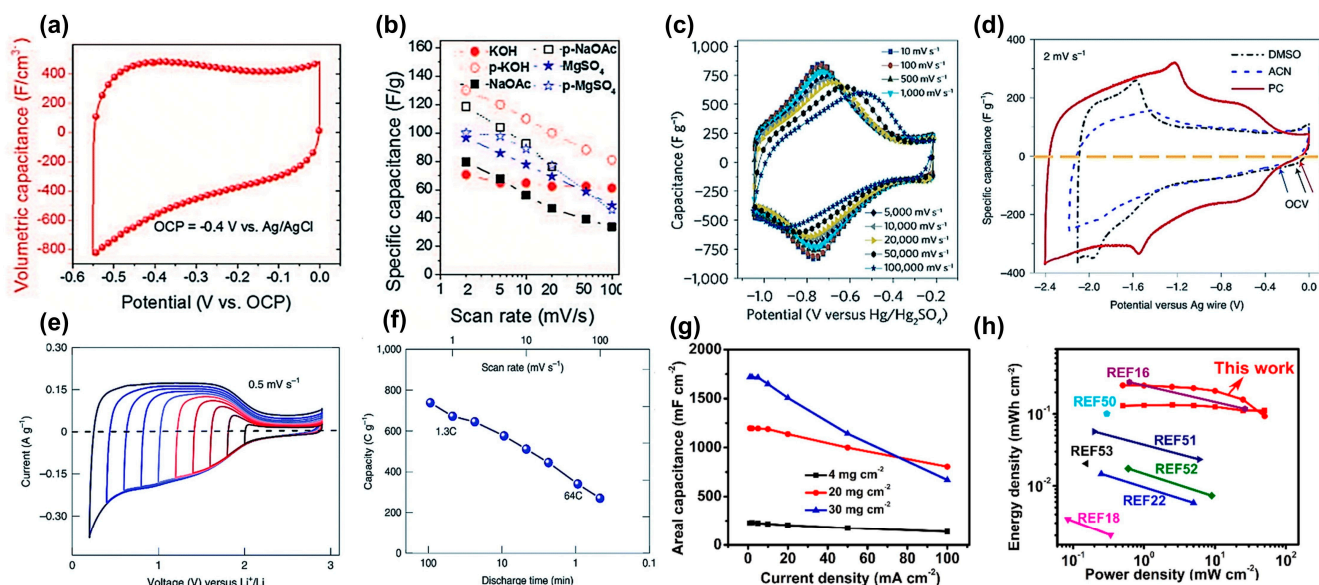


Figure 11. (a) Cyclic voltammetry (CV) curve of $\text{Ti}_3\text{C}_2\text{T}_x$ paper in KOH electrolyte. (b) Rate performance of $\text{Ti}_3\text{C}_2\text{T}_x$ paper (open symbols) versus multilayered exfoliated $\text{Ti}_3\text{C}_2\text{T}_x$ electrodes (solid symbols) in various electrolytes. Reproduced with permission [90]. Copyright 2013, American Chemical Society. The American Association for the Advancement of Science. (c) Cyclic voltammetry data were collected at scan rates from 10 to 100,000 mV s^{-1} in 3 M H_2SO_4 . Reproduced with permission [153]. Copyright 2017, Macmillan Publishers Limited, part of Springer Nature. (d) CV curves of a $\text{Ti}_3\text{C}_2\text{T}_x$ electrode with 1 M LiTFSI in DMSO, can, and PC organic electrolytes. Reproduced with permission [154]. Copyright 2019, Springer Nature. (e) CV curves of the $\text{Ti}_3\text{C}_2\text{T}_x$ electrode in 1 M LiPF_6 (in 1:1 ethylene carbonate/dimethyl carbonate) electrolyte. (f) $\text{Ti}_3\text{C}_2\text{T}_x$ electrode capacity versus discharge time from CV curves recorded at various potential scan rates. Reproduced with permission [83]. Copyright 2020, Springer Nature. (g) A summary of FT-SSSs areal capacitance under different charging/discharging current densities. (h) Ragone plot of FT-SSS in comparison to other state-of-the-art MXene-based SSSs. Reproduced with permission [155]. Copyright 2022, Elsevier.

5.2. Neutral Electrolytes

Similarly to their performance in a KOH electrolyte, the capacitive behavior of $\text{Ti}_3\text{C}_2\text{T}_x$ MXenes in neutral electrolytes is primarily governed by their electric double-layer capacitance (EDLC) [156]. Hu et al. conducted studies demonstrating that a $\text{Ti}_3\text{C}_2\text{T}_x$ electrode exhibited only electric double-layer capacitance in $(\text{NH}_4)_2\text{SO}_4$ or MgSO_4 solution electrolytes, with capacitance values lower than those observed in acidic electrolytes [157]. Gao et al. reported on a vanadium (V)-doped $\text{Ti}_3\text{C}_2\text{T}_x$ electrode with a gravimetric capacitance of 365.9 F g^{-1} in a 2 M potassium chloride (KCl) electrolyte [158]. However, this capacitance was lower than that of a 3 mm $\text{Ti}_3\text{C}_2\text{T}_x$ hydrogel electrode in 3 M H_2SO_4 (which was approximately 380 F g^{-1}) [153]. In the 2 M KCl electrolyte, the V-doped $\text{Ti}_3\text{C}_2\text{T}_x$ electrode exhibited a voltage range of 0.7 V, and no significant redox peaks were observed in its cyclic voltammetry curves, indicating the EDLC behavior in a neutral electrolyte [158].

5.3. Acidic Electrolytes

The utilization of an H_2SO_4 electrolyte in supercapacitors offers several advantages, including the presence of protons (the smallest cations) and excellent conductivity. These factors facilitate rapid surface redox reactions in transition-metal compounds. In a study by Ghidiu et al., free-standing, flexible $\text{Ti}_3\text{C}_2\text{T}_x$ electrodes were assembled into supercapacitors using a 1 M H_2SO_4 electrolyte, resulting in volumetric capacitances of up to 900 F cm^{-3} and a gravimetric capacitance of 245 F g^{-1} , surpassing the capacitance achieved in KOH electrolyte [6]. Lukatskaya et al. reported a $\text{Ti}_3\text{C}_2\text{T}_x$ electrode on a glassy carbon current collector with a potential range of -0.9 V in 3 M H_2SO_4 (Figure 11c). Notably, the $\text{Ti}_3\text{C}_2\text{T}_x$

hydrogel exhibited volumetric capacitances of up to 1500 F cm^{-3} in $3 \text{ M H}_2\text{SO}_4$ [153]. The higher concentration of protons in $3 \text{ M H}_2\text{SO}_4$ compared to $1 \text{ M H}_2\text{SO}_4$ could contribute to this enhanced volumetric capacitance, while the enlarged potential range could be attributed to the weak hydrogen evolution reaction occurring on the glassy carbon electrode. The high capacitance observed in the H_2SO_4 electrolyte is likely related to a pseudocapacitive energy storage mechanism, as evidenced by the presence of redox peaks in the cyclic voltammetry curves and changes in the chemical valence state of titanium [159]. In situ X-ray diffraction showed the lattice's shrinkage during the charging process from 0 V to -0.6 V versus Ag/AgCl and subsequent expansion from -0.6 V to -0.9 V versus Ag/AgCl , demonstrating the pseudo-intercalation energy storage mechanism of $\text{Ti}_3\text{C}_2\text{T}_x$ in a H_2SO_4 electrolyte [160]. Hu et al. investigated the electrochemical behavior of a $\text{Ti}_3\text{C}_2\text{T}_x$ electrode in an H_2SO_4 electrolyte through in situ electrochemical Raman spectroscopy, which revealed a bonding and debonding of hydronium with its terminal O groups during discharge and charge, respectively [157]. Additionally, this reversible bonding/debonding process contributed to the valence change of the Ti element in $\text{Ti}_3\text{C}_2\text{T}_x$, further enhancing the electrode's pseudocapacitance in the H_2SO_4 electrolyte.

5.4. Organic Electrolytes

In addition to aqueous electrolytes, organic electrolytes have also been extensively investigated due to their larger voltage windows, which enable higher energy densities. Organic electrolytes show promise for operating across wider potential ranges. Suitable organic electrolytes for $\text{Ti}_3\text{C}_2\text{T}_x$ MXene electrodes facilitate the insertion reaction of ions between their layers. Wang et al. conducted a study where the $\text{Ti}_3\text{C}_2\text{T}_x$ electrode exhibited a potential window of 2.4 V in a lithium-containing electrolyte, specifically lithium bis(trifluoromethylsulfonyl) amine (LiTFSI) with propylene carbonate (PC) as the solvent [154]. Moreover, the $\text{Ti}_3\text{C}_2\text{T}_x$ electrode demonstrated a capacitance of 195 F g^{-1} at a scan rate of 2 mV s^{-1} in the LiTFSI-PC electrolyte, surpassing that of the LiTFSI-DMSO (130 F g^{-1}) and LiTFSI-CAN (110 F g^{-1}) electrolytes. This improvement can be attributed to the more efficient desolvation of lithium ions in the PC system (Figure 11d). Li et al. reported the fabrication of a $\text{Ti}_3\text{C}_2\text{T}_x$ electrode through the Lewis acidic molten salt-etching method, which showed a potential window of 2.8 V in a 1 M LiPF_6 carbonate-based electrolyte. The system exhibited storage capacities of up to 738 C g^{-1} (264 F g^{-1}) at a scan rate of 0.5 mV s^{-1} (Figure 11e,f) [83]. Luo et al. demonstrated that a $\text{Ti}_3\text{C}_2\text{T}_x$ electrode had an applied potential range of 3.0 V in a 1 M NaClO_4 carbonate-based electrolyte [161]. In organic electrolytes, $\text{Ti}_3\text{C}_2\text{T}_x$ electrodes typically exhibit a potential window of $>2.0 \text{ V}$, which is wider than those obtained in aqueous electrolytes [162].

5.5. Solid Electrolytes

Liu et al. reported the improved performance of MXene-based SSS from a new perspective, using a freeze-thawed MSA/PVA hydrogel electrolyte with high ionic conductivity and low-temperature resistance [155]. The FT-SSS presents a high rate capability that exceeds corresponding aqueous AQSs. As shown in Figure 11g, its areal capacitance reaches 1719 mF cm^{-2} . It also presents low-temperature resistance, long cycling stability, and good flexibility. The advanced electrolyte and the existence of MSA contribute to its performance, which is far superior to that seen in other studies (Figure 11h). During casting, the MSA/MSA ions pre-intercalate into MXene and result in a wrinkled and porous structure that reduces the stacking effect of MXene and enhances electrolyte accessibility. Its -OH and H_2O (physisorbed to-OH) content rises so that its pseudocapacitance is enhanced. With this improvement of the high ionic conductivity of the MSA/PVA hydrogel, the dynamic of the device is greatly enhanced. This research presents a new perspective for improving MXene-based solid-state supercapacitors' performances by fabricating MSA/PVA electrolytes and may provide more possibilities for future investigations into solid-state supercapacitors.

Table 4 summarizes the effects of different electrolytes on the performance of MXene and MXene-based supercapacitors. In general, ions with smaller radii or hydration shells

will lead to a higher capacitance. The hydronium ions in H_2SO_4 with the smallest hydration radii can access a larger number of electrochemically active sites between the $Ti_3C_2T_x$ layers, which may be one of the possible reasons why a higher capacitance is achieved in acidic electrolytes. However, aqueous electrolytes face the shortcoming of a limited voltage window since hydrogen and oxygen evolution reactions generally occur in aqueous electrolytes at a potential higher than 1.23 V (1.23 V is the decomposition voltage of water), which suppresses their applications in high-voltage and high-energy-density systems.

Table 4. The effects of different electrolytes on the supercapacitor properties of MXene and MXene-based electrodes.

Materials	Electrolyte	Volumetric Capacitance ($F\text{ cm}^{-3}$)	Gravimetric Capacitance ($F\text{ g}^{-1}$)	Areal Capacitance ($mF\text{ cm}^{-2}$)	Cycling Stability	Flexibility	Ref.
$Ti_3C_2T_x/OMC$	3 M KOH	823 (1 A g^{-1})	329 (1 A g^{-1})	No mention	117% retention (100 mV s^{-1}), 10,000 cycles	No mention	[163]
$Ti_3C_2T_x/NiCo_2S_4$	3 M KOH	No mention	1147.47 (1 A g^{-1})	No mention	91.1% retention (10 A g^{-1}), 3000 cycles	No mention	[164]
$Ti_3C_2T_x$	2M KCl	No mention	365.9 (2 mV s^{-1})	No mention	95% retention (10 A g^{-1}), 5000 cycles	No mention	[158]
$Ti_3C_2T_x/CNT$	$MgSO_4$	390 (20 mV s^{-1})	~ 125 (2 mV s^{-1})	No mention	$\sim 100\%$ retention (5 A g^{-1}), 10,000 cycles	Flexible film	[165]
$Ti_3C_2T_x/rGO$	3 M H_2SO_4	1040 (2 mV s^{-1})	335 (2 mV s^{-1})	No mention	$\sim 100\%$ retention (100 mV s^{-1}), 20,000 cycles	Flexible film	[166]
$Ti_3C_2T_x/PPy$	0.5 M H_2SO_4	406 (30 mV s^{-1})	No mention	203 (30 mV s^{-1})	$\sim 100\%$ retention, 20,000 cycles	Bending angles: $60^\circ, 90^\circ, 150^\circ$	[167]
$Ti_3C_2T_x$	3 M H_2SO_4	1500 (2 mV s^{-1})	380 (2 mV s^{-1})	4000 (2 mV s^{-1})	Over 90% retention (10 A g^{-1}), 10,000 cycles	Flexible film	[157]
$Ti_3C_2T_x$	MSA/PVA hydrogel	No mention	No mention	1719 (2 mV s^{-1})	92% retention (10 A g^{-1}), 80,000 cycles	Bending angles: $0^\circ\text{--}180^\circ$	[155]
$Ti_3C_2T_x$	LiTFSI-PC	410 (2 mV s^{-1})	195 (2 mV s^{-1})	No mention	94% retention (100 mV s^{-1}), 10,000 cycles	No mention	[154]

6. Summary and Outlook

6.1. Summary

In summary, since its inception, MXene has experienced rapid development because of its distinctive two-dimensional structure, excellent hydrophilicity, conductivity, tunable surface chemistry, outstanding flexibility, and ion intercalation properties. With researchers further exploring the applications of MXene materials in various scientific fields, their use in the sphere of supercapacitors' chemical energy storage continues to evolve. This review article has outlined the basic construction and characteristics of MXene, its preparation methods, and the application of MXene composite materials in supercapacitors, detailing the latest research on different types of MXene-based composite materials and their supercapacitor applications.

6.2. Outlook

When looking at the research on MXene-based composite materials in supercapacitors, the challenges and opportunities in this field mainly include the following:

1. The preparation methods used to make MXene still primarily rely on etching, whether acid etching or alkaline etching, and especially HF etching, which is dangerous and involves handling strong corrosive substances such as waste acids and alkalis. These methods are polluting, low-yielding, and expensive. Although direct synthesis methods have been proven effective in preparing MXene and avoiding the generation of pollutants, their production yield still needs to be improved. Therefore, new MXene preparation processes need to be developed to transition from the laboratory to production on a larger scale and, eventually, commercialized operations.
2. The energy density of MXene remains relatively low, so it is necessary to enhance the structural design of MXene by enlarging and utilizing the space between each of its layers, matching the radius of the ions diffused in the electrolyte as much as possible, maximize the energy storage performance of MXene, establish the influence of MXene's structure on its energy storage mechanisms, and guide the subsequent structural design of MXene electrodes.
3. Different types of MXene composite materials have unique characteristics. For example, MXene/carbon composites offer advantages in terms of their high specific capacitance and cycling stability in supercapacitors, but their energy density and conductivity are limited. MXene/metal oxide composites have a higher specific capacitance, but their cycling capability and power density are still limited due to their poor electrochemical kinetics. MXene/metal hydroxide composites effectively reduce the self-stacking effect of MXene, improving the electrochemical performance of the electrode. However, they also have some limitations to their energy density and conductivity. MXene/conductive polymer composites effectively suppress layer stacking, increase the exposure of the active surface, and facilitate electron transfer and rapid reactions while improving the mechanical properties and stability of the material. However, the energy density of conductive polymers is typically lower, limiting their use in supercapacitors intended for certain high-energy density applications. Therefore, further research and improvements are needed.
4. The preparation of MXene-based composite materials is an effective means to improve the energy storage performance of MXene, but the selection of the materials used in these composites still lacks specificity. Therefore, in the creation of composite materials using MXene, selecting heteromaterials with excellent energy storage performance remains a necessary research direction for alleviating the impact of the self-stacking of MXene and synergistically improving the material's energy storage performance.
5. The easy oxidation of MXene remains a significant factor limiting the application of MXene supercapacitors. Enhancing the thermal stability and electrochemical stability of MXene by adding other substances and preparing MXene-based composites is also an important topic in the study of MXene-based capacitors.
6. Wearable electronic devices are a growing trend, and developing flexible electrodes is an important part of the research in this area. Further research is needed to prepare flexible, miniaturized, and cost-effective supercapacitor devices.

Author Contributions: Writing—Original Draft Preparation, M.S.; Funding Acquisition, M.S.; Validation, W.Y.; Formal Analysis, M.S. and W.Y.; Data Curation, J.Z. and K.Z.; Writing—Review & Editing, M.S. All authors have read and agreed to the published version of the manuscript.

Funding: This work was financially supported by the Fundamental Research Funds for the Central Universities (FRF-IDRY-22-030) and the Teaching Reformation Project of Undergraduate Education at the University of Science and Technology Beijing (JG2021Z07).

Data Availability Statement: No new data were created or analyzed in this study. Data sharing is not applicable to this article.

Conflicts of Interest: The authors declare no conflicts of interest.

References

1. Lin, Z.; Li, L.; Xi, C.; Li, X.; Feng, S.; Wang, C.; Wang, H.; Li, T.; Ma, Y. Fabrication of the hollow dodecahedral NiCoZn layered double hydroxide for high-performance flexible asymmetric supercapacitor. *J. Colloid Interface Sci.* **2024**, *657*, 91–101. [[CrossRef](#)] [[PubMed](#)]
2. Chen, Y.; Yang, H.; Han, Z.; Bo, Z.; Yan, J.; Cen, K.; Ostrikov, K.K. MXene-Based Electrodes for Supercapacitor Energy Storage. *Energy Fuels* **2022**, *36*, 2390–2406. [[CrossRef](#)]
3. Wei, J.; Sajjad, M.; Zhang, J.; Li, D.; Mao, Z. The rise of novel 2D materials beyond graphene: A comprehensive review of their potential as supercapacitor electrodes. *Surf. Interfaces* **2023**, *42*, 103334. [[CrossRef](#)]
4. Sahoo, B.B.; Pandey, V.S.; Dogonchi, A.S.; Mohapatra, P.K.; Thatoi, D.N.; Nayak, N.; Nayak, M.K. A state-of-art review on 2D material-boosted metal oxide nanoparticle electrodes: Supercapacitor applications. *J. Energy Storage* **2023**, *65*, 107335. [[CrossRef](#)]
5. Rohith, R.; Prasannakumar, A.T.; Mohan, D.R.R.; Manju, V.; Varma, D.S.J. Advances in 2D Molybdenum Disulfide-Based Functional Materials for Supercapacitor Applications. *ChemistrySelect* **2022**, *7*, e202203068.
6. Ghidui, M.; Lukatskaya, M.R.; Zhao, M.-Q.; Gogotsi, Y.; Barsoum, M.W. Conductive two-dimensional titanium carbide ‘clay’ with high volumetric capacitance. *Nature* **2014**, *516*, 78–81. [[CrossRef](#)] [[PubMed](#)]
7. Zhao, S.; Chen, C.; Zhao, X.; Chu, X.; Du, F.; Chen, G.; Gogotsi, Y.; Gao, Y.; Dall, Y. Flexible Nb₄C₃T_x Film with Large Interlayer Spacing for High-Performance Supercapacitors. *Adv. Funct. Mater.* **2020**, *30*, 2000815. [[CrossRef](#)]
8. Xu, P.; Xiao, H.; Liang, X.; Zhang, T.; Zhang, F.; Liu, C.; Lang, B.; Gao, Q. A MXene-based EDA-Ti₃C₂T_x intercalation compound with expanded interlayer spacing as high performance supercapacitor electrode material. *Carbon* **2021**, *173*, 135–144. [[CrossRef](#)]
9. Naguib, M.; Kurtoglu, M.; Presser, V.; Lu, J.; Niu, J.; Heon, M.; Hultman, L.; Gogotsi, Y.; Barsoum, M.W. Two-Dimensional Nanocrystals Produced by Exfoliation of Ti₃AlC₂. *Adv. Mater.* **2011**, *23*, 4248–4253. [[CrossRef](#)]
10. Zhang, X.; Javed, M.S.; Ali, S.; Ahmad, A.; Shah, S.S.A.; Hussain, I.; Choi, D.; Tighezza, A.M.; Tag-Eldin, E.; Xia, C.; et al. Band engineering in Ti₂N/Ti₃C₂T_x-MXene interface to enhance the performance of aqueous NH₄⁺-ion hybrid supercapacitors. *Nano Energy* **2024**, *120*, 109108. [[CrossRef](#)]
11. Soundiraraju, B.; George, B.K. Two-Dimensional Titanium Nitride (Ti₂N) MXene: Synthesis, Characterization, and Potential Application as Surface-Enhanced Raman Scattering Substrate. *ACS Nano* **2017**, *11*, 8892–8900. [[CrossRef](#)] [[PubMed](#)]
12. Naguib, M.; Unocic, R.R.; Armstrong, B.L.; Nanda, J. Large-scale delamination of multi-layers transition metal carbides; carbonitrides “MXenes”. *Dalton Trans.* **2015**, *44*, 9353–9358. [[CrossRef](#)] [[PubMed](#)]
13. Vattikuti, S.V.P.; Shim, J.; Rosaiah, P.; Mauger, A.; Julien, C.M. Recent Advances and Strategies in MXene-Based Electrodes for Supercapacitors: Applications, Challenges and Future Prospects. *Nanomaterials* **2024**, *14*, 62. [[CrossRef](#)] [[PubMed](#)]
14. Alli, Y.A.; Bamisaye, A.; Nancy, P.; Zachariah, S.M.; Oladoye, P.O.; Bankole, O.M.; Akamo, D.O.; Chkirida, S.; Anuar, H.; Thomas, S. MXene composites: Properties, synthesis and its emerging application in rechargeable batteries. *J. Energy Storage* **2024**, *77*, 109954. [[CrossRef](#)]
15. Xu, H.; Dong, H.; Liu, X.; Qiao, H.; Chen, G.; Du, F.; Dall’Agnese, Y.; Gao, Y. High-Temperature Oxidized Mo₂CT_x MXene for a High-Performance Supercapacitor. *ACS Appl. Mater. Interfaces* **2023**, *15*, 53549–53557. [[CrossRef](#)] [[PubMed](#)]
16. Weng, M.; Zhou, J.; Ye, Y.; Qiu, H.; Zhou, P.; Luo, Z.; Guo, Q. Self-chargeable supercapacitor made with MXene-bacterial cellulose nanofiber composite for wearable devices. *J. Colloid Interface Sci.* **2023**, *647*, 277–286. [[CrossRef](#)] [[PubMed](#)]
17. Otgonbayar, Z.; Yang, S.; Kim, I.-J.; Oh, W.-C. Recent advances in 2D MXene and solid state electrolyte for energy storage applications: Comprehensive review. *Chem. Eng. J.* **2023**, *472*, 144801. [[CrossRef](#)]
18. Gandla, D.; Zhuang, Z.; Jadhav, V.V.; Tan, D.Q. Lewis acid molten salt method for 2D MXene synthesis and energy storage applications: A review. *Energy Storage Mater.* **2023**, *63*, 102977. [[CrossRef](#)]
19. Fu, X.-Y.; Shu, R.-Y.; Ma, C.-J.; Zhang, Y.-Y.; Jiang, H.-B.; Yao, M.-N. Self-assembled MXene-graphene oxide composite enhanced laser-induced graphene based electrodes towards conformal supercapacitor applications. *Appl. Surf. Sci.* **2023**, *631*, 157549. [[CrossRef](#)]
20. Kim, M.C.; Saeed, G.; Alam, A.; Choi, Y.; Zhang, L.; Lee, D.; Kwon, S.H.; Mathur, S.; Kim, K.H. Ultrafine nanoparticles of tin-cobalt-sulfide decorated over 2D MXene sheets as a cathode material for high-performance asymmetric supercapacitor. *J. Ind. Eng. Chem.* **2023**, *124*, 294–303.
21. Jimmy, J.; Kandasubramanian, B. Mxene functionalized polymer composites: Synthesis and applications. *Eur. Polym. J.* **2020**, *122*, 109367. [[CrossRef](#)]
22. Meng, Y.; Zhang, Z.; Hou, X.; Wang, T.; Guo, X.; Liu, X.; Tian, M.; Qu, L.; Zhang, X. Flexible and ultra-thin graphene@MXene@Fe₃O₄ composites with excellent microwave absorption performance. *Ceram. Int.* **2024**, *50*, 6624–6633. [[CrossRef](#)]
23. Amani, A.M.; Tayebi, L.; Abbasi, M.; Vaez, A.; Kamyab, H.; Chelliapan, S.; Vafa, E. The Need for Smart Materials in an Expanding Smart World: MXene-Based Wearable Electronics and Their Advantageous Applications. *ACS Omega* **2024**, *9*, 3123–3142. [[CrossRef](#)]
24. Li, H.; Fan, K.; Xiong, P.; Zhou, H.; Lin, Z.; Tao, K.; Liu, T.; Guo, X.; Zhu, Y.; Zhuang, L.; et al. Selective grafting of phosphorus onto Ti₃C₂T_x MXene enables a two-proton process and enhanced charge storage. *J. Mater. Chem. A* **2024**, *12*, 3449–3459. [[CrossRef](#)]
25. Zheng, W.; Yang, L.; Wang, L.; Pan, L.; Zhang, P.; Sun, Z. MXene nanomesh for high-performance supercapacitor. *J. Alloys Compd.* **2024**, *976*, 173065. [[CrossRef](#)]
26. Ahmad, R.; Iqbal, N.; Noor, T.; Nemani, S.K.; Zhu, L.; Anasori, B. Metal–Organic Framework/Ti₃C₂T_x MXene-Derived Functional Nanostructures for High-Performance Supercapacitors. *ACS Appl. Nano Mater.* **2024**, *7*, 253–266. [[CrossRef](#)]

27. Paul, T.K.; Parvez, M.S.; Ahmed, C.M. Recent Progress and Prospects of MXene/Cellulose-Based Composite Electrodes: A Sustainable Pathway towards Supercapacitor Application. *ChemElectroChem* **2024**, *11*, e202300435. [[CrossRef](#)]
28. Khan, U.; Gao, B.; Kong, L.B.; Chen, Z.; Que, W. Green synthesis of fluorine-free MXene via hydrothermal process: A sustainable approach for proton supercapacitor electrodes. *Electrochim. Acta* **2024**, *475*, 143651. [[CrossRef](#)]
29. Naguib, M.; Mochalin, V.N.; Barsoum, M.W.; Gogotsi, Y. 25th Anniversary Article: MXenes: A New Family of Two-Dimensional Materials. *Adv. Mater.* **2014**, *26*, 992–1005. [[CrossRef](#)]
30. Jin, X.; Zhang, B.; Dong, L.; Li, X.; Liu, D.; Hou, S.; Zhang, Y.; Niu, H.; Zhang, F.-M. MXene-derived composite catalyst with micro-holes by a solvothermal method with tiny amount of solvent for high-efficiency catalytic hydrogen production. *Int. J. Hydrogen Energy* **2024**, *51*, 1161–1169. [[CrossRef](#)]
31. Kalidasan, B.; Pandey, A.K.; Saidur, R.; Han, T.K.; Mishra, Y.N. MXene-based eutectic salt hydrate phase change material for efficient thermal features, corrosion resistance & photo-thermal energy conversion. *Mater. Today Sustain.* **2024**, *25*, 100634.
32. Tang, Q.; Zhou, Z.; Shen, P. Are MXenes Promising Anode Materials for Li Ion Batteries Computational Studies on Electronic Properties and Li Storage Capability of Ti_3C_2 and $Ti_3C_2X_2$ ($X = F, OH$) Monolayer. *J. Am. Chem. Soc.* **2012**, *134*, 16909–16916. [[CrossRef](#)]
33. Liang, C.; Meng, Y.; Zhang, Y.; Zhang, H.; Wang, W.; Lu, M.; Wang, G. Insights into the impact of interlayer spacing on MXene-based electrodes for supercapacitors: A review. *J. Energy Storage* **2023**, *65*, 107341. [[CrossRef](#)]
34. Levitt, A.S.; Alhabeab, M.; Hatter, C.B.; Sarycheva, A.; Dionb, G.; Gogotsi, Y. Electrospun MXene/carbon nanofibers as supercapacitor electrodes. *J. Mater. Chem. A* **2019**, *7*, 269–277. [[CrossRef](#)]
35. Tian, Y.; Ju, M.; Luo, Y.; Bin, X.; Lou, X.; Que, W. In situ oxygen doped $Ti_3C_2T_x$ MXene flexible film as supercapacitor electrode. *Chem. Eng. J.* **2022**, *446*, 137451. [[CrossRef](#)]
36. Wang, X.; Bak, S.-M.; Han, M.; Shuck, C.E.; McHugh, C.; Li, K.; Li, J.; Tang, J.; Gogotsi, Y. Surface Redox Pseudocapacitance of Partially Oxidized Titanium Carbide MXene in Water-in-Salt Electrolyte. *ACS Energy Lett.* **2022**, *7*, 30–35. [[CrossRef](#)]
37. Ma, R.; Zhang, X.; Zhuo, J.; Cao, L.; Song, Y.; Yin, Y.; Wang, X.; Yang, G.; Yi, F. Self-Supporting, Binder-Free, and Flexible $Ti_3C_2T_x$ MXene-Based Supercapacitor Electrode with Improved Electrochemical Performance. *ACS Nano* **2022**, *16*, 9713–9727. [[CrossRef](#)]
38. Cai, M.; Wei, X.; Huang, H.; Yuan, F.; Li, C.; Xu, S.; Liang, X.; Zhou, W.; Guo, J. Nitrogen-doped $Ti_3C_2T_x$ MXene prepared by thermal decomposition of ammonium salts and its application in flexible quasi-solid-state supercapacitor. *Chem. Eng. J.* **2023**, *458*, 141338. [[CrossRef](#)]
39. Kawai, K.; Fujita, M.; Iizuka, R.; Yamada, A.; Okubo, M. Influence of surface termination groups on electrochemical charge storage of MXene electrodes. *2D Mater.* **2023**, *10*, 014012. [[CrossRef](#)]
40. Ma, R.; Chen, Z.; Zhao, D.; Zhang, X.; Zhuo, J.; Yin, Y.; Wang, X.; Yang, G.; Yi, F. $Ti_3C_2T_x$ MXene for electrode materials of supercapacitors. *J. Mater. Chem. A* **2021**, *9*, 11501–11529. [[CrossRef](#)]
41. Zhang, J.; Kong, N.; Hegh, D.; Usman, K.A.S.; Guan, G.; Qin, S.; Jurewicz, I.; Yang, W.; Razal, J.M. Freezing Titanium Carbide Aqueous Dispersions for Ultra-long-term Storage. *ACS Appl. Mater. Interfaces* **2020**, *12*, 34032–34040. [[CrossRef](#)]
42. De, S.; Maity, C.K.; Sahoo, S.; Nayak, G.C. Polyindole Booster for $Ti_3C_2T_x$ MXene Based Symmetric and Asymmetric Supercapacitor Devices. *ACS Appl. Energy Mater.* **2021**, *4*, 3712–3723. [[CrossRef](#)]
43. Sun, S.; Zhu, X.; Wu, X.; Xu, M.; Hu, Y.; Bao, N.; Wu, G. Covalent-architected molybdenum disulfide arrays on $Ti_3C_2T_x$ MXene fiber towards robust capacitive energy storage. *J. Mater. Sci. Technol.* **2023**, *139*, 23–30. [[CrossRef](#)]
44. Kasprzak, D.; Mayorga-Martinez, C.C.; Alduhaish, O.; Pumera, M. Wearable and Flexible All-Solid-State Supercapacitor Based on MXene and Chitin. *Energy Technol.* **2023**, *11*, 2201103. [[CrossRef](#)]
45. De, S.; Maity, C.K.; Kim, M.J.; Nayak, G.C. Tin(IV) selenide anchored-biowaste derived porous carbon- $Ti_3C_2T_x$ (MXene) nanohybrid: An ionic electrolyte enhanced high performing flexible supercapacitor electrode. *Electrochim. Acta* **2023**, *463*, 142811. [[CrossRef](#)]
46. Karim, G.M.; Dutta, P.; Majumdar, A.; Patra, A.; Deb, S.K.; Das, S.; Dambhare, N.V.; Rath, A.K.; Maiti, U.N. Ultra-fast electro-reduction and activation of graphene for high energy density wearable supercapacitor asymmetrically designed with MXene. *Carbon* **2023**, *203*, 191–201. [[CrossRef](#)]
47. Lorencova, L.; Kasak, P.; Kosutova, N.; Jerigova, M.; Noskovicova, E.; Vikartovska, A.; Barath, M.; Farkas, P.; Tkac, J. MXene-based electrochemical devices applied for healthcare applications. *Microchim. Acta* **2024**, *191*, 88. [[CrossRef](#)]
48. Zeraati, A.S.; Mirkhani, S.A.; Sun, P.; Naguib, M.; Braun, P.V.; Sundararaj, U. Improved synthesis of $Ti_3C_2T_x$ MXenes resulting in exceptional electrical conductivity, high synthesis yield, and enhanced capacitance. *Nanoscale* **2021**, *13*, 3572–3580. [[CrossRef](#)]
49. Mathis, T.S.; Maleski, K.; Goad, A.; Sarycheva, A.; Anayee, M.; Foucher, A.C.; Hantanasirisakul, K.; Shuck, C.E.; Stach, E.A.; Gogotsi, Y. Modified MAX Phase Synthesis for Environmentally Stable and Highly Conductive Ti_3C_2 MXene. *ACS Nano* **2021**, *15*, 6420–6429. [[CrossRef](#)]
50. Jia, L.; Zhou, S.; Ahmed, A.; Yang, Z.; Liu, S.; Wang, H.; Li, F.; Zhang, M.; Zhang, Y.; Sun, L. Tuning MXene electrical conductivity towards multifunctionality. *Chem. Eng. J.* **2023**, *475*, 146361. [[CrossRef](#)]
51. Zhang, J.; Kong, N.; Uzun, S.; Levitt, A.; Seyedin, S.; Lynch, P.A.; Qin, S.; Han, M.; Yang, W.; Liu, J.; et al. Scalable Manufacturing of Free-Standing, Strong $Ti_3C_2T_x$ MXene Films with Outstanding Conductivity. *Adv. Mater.* **2020**, *32*, 2001093. [[CrossRef](#)]
52. Aravind, A.M.; Tomy, M.; Kuttapan, A. Ann Mary Kakkassery Aippunny, Xavier Thankappan Suryabai, Progress of 2D MXene as an Electrode Architecture for Advanced Supercapacitors: A Comprehensive Review. *ACS Omega* **2023**, *8*, 44375–44394. [[CrossRef](#)]

53. Bai, Y.; Liu, C.; Chen, T.; Li, W.; Zheng, S.; Pi, Y.; Luo, Y.; Pang, H. MXene-Copper/Cobalt Hybrids via Lewis Acidic Molten Salts Etching for High Performance Symmetric Supercapacitors. *Angew. Chem. Int. Ed.* **2021**, *60*, 25318–25322. [[CrossRef](#)]
54. Lu, Q.; Liu, C.; Zhao, Y.; Pan, W.; Xie, K.; Yue, P.; Zhang, G.; Omar, A.; Liu, L.; Yu, M.; et al. Freestanding MXene-based macroforms for electrochemical energy storage applications. *Susmat* **2023**, *3*, 471–497. [[CrossRef](#)]
55. Garg, R.; Agarwal, A.; Agarwal, M. Effect of vanadium doping on MXene-based supercapacitor. *J. Mater. Sci. Mater. Electron.* **2021**, *32*, 22046–22059. [[CrossRef](#)]
56. Jiang, Q.; Lei, Y.; Liang, H.; Xi, K.; Xia, C.; Alshareef, H.N. Review of MXene electrochemical microsupercapacitors. *Energy Storage Mater.* **2020**, *27*, 78–95. [[CrossRef](#)]
57. Zhang, Y.-Z.; El-Demellawi, J.K.; Jiang, Q.; Ge, G.; Liang, H.; Lee, K.; Dong, X.; Alshareef, H.N. MXene hydrogels: Fundamentals and applications. *Chem. Soc. Rev.* **2020**, *49*, 7229–7251. [[CrossRef](#)]
58. Idumah, C.I. Influence of surfaces and interfaces on MXene and MXene hybrid polymeric nanoarchitectures, properties, and applications. *J. Mater. Sci.* **2022**, *57*, 14579–14619. [[CrossRef](#)]
59. Xiong, D.; Li, X.; Bai, Z.; Lu, S. Recent Advances in Layered $Ti_3C_2T_x$ MXene for Electrochemical Energy Storage. *Small* **2018**, *14*, 1703419. [[CrossRef](#)]
60. Song, F.; Li, G.; Zhu, Y.; Wu, Z.; Xie, X.; Zhang, N. Rising from the horizon: Three-dimensional functional architectures assembled with MXene nanosheets. *J. Mater. Chem. A* **2020**, *8*, 18538–18559. [[CrossRef](#)]
61. Yang, Q.; Wang, Y.; Li, X.; Li, H.; Wang, Z.; Tang, Z.; Ma, L.; Mo, F.; Zhi, C. Recent Progress of MXene-Based Nanomaterials in Flexible Energy Storage and Electronic Devices. *Energy Environ. Mater.* **2018**, *1*, 183–195. [[CrossRef](#)]
62. Luo, Y.; Que, W.; Bin, X.; Xia, C.; Kong, B.; Gao, B.; Kong, L.B. Flexible MXene-Based Composite Films: Synthesis, Modification, and Applications as Electrodes of Supercapacitors. *Small* **2022**, *18*, 2201290. [[CrossRef](#)] [[PubMed](#)]
63. Panda, S.; Deshmukh, K.; Pasha, S.K.K.; Theerthagiri, J.; Manickam, S.; Choi, M.Y. MXene based emerging materials for supercapacitor applications: Recent advances, challenges, and future perspectives. *Coord. Chem. Rev.* **2022**, *462*, 214518. [[CrossRef](#)]
64. Mazhar, S.; Qarni, A.A.; Haq, Y.U.; Haq, Z.U.; Murtaza, I. Promising PVC/MXene based flexible thin film nanocomposites with excellent dielectric, thermal and mechanical properties. *Ceram. Int.* **2020**, *46*, 12593–12605. [[CrossRef](#)]
65. Tang, B.; Yang, Y.; Shi, Y.; Nie, H.; Xia, H.; Shen, X. Improved mechanical performances of short aramid fiber-reinforced polypropylene composites by Ti_3C_2 MXene nanosheets. *Polym. Compos.* **2021**, *42*, 2010–2018. [[CrossRef](#)]
66. Chu, N.; Luo, C.; Chen, X.; Li, L.; Liang, C.; Chao, M.; Yan, L. $Ti_3C_2T_x$ MXene/polyimide composites film with excellent mechanical properties and electromagnetic interference shielding properties. *J. Alloys Compd.* **2023**, *955*, 170241. [[CrossRef](#)]
67. Shekhirev, M.; Shuck, C.E.; Sarycheva, A.; Gogotsi, Y. Characterization of MXenes at every step, from their precursors to single flakes and assembled films. *Prog. Mater. Sci.* **2021**, *120*, 100757. [[CrossRef](#)]
68. Guo, Z.; Zhou, J.; Si, C.; Sun, Z. Flexible two-dimensional $Ti_{n+1}C_n$ ($n = 1, 2$ and 3) and their functionalized MXenes predicted by density functional theories. *Phys. Chem. Chem. Phys.* **2015**, *17*, 15348–15354. [[CrossRef](#)]
69. Iravani, S.; Rabiee, N.; Makvandi, P. Advancements in MXene-based composites for electronic skins. *J. Mater. Chem. B* **2024**, *12*, 895–915. [[CrossRef](#)]
70. Sun, J.; Liu, Y.; Huang, J.; Li, J.; Chen, M.; Hu, X.; Liu, Y.; Wang, R.; Shen, Y.; Li, J.; et al. Size-refinement enhanced flexibility and electrochemical performance of MXene electrodes for flexible waterproof supercapacitors. *J. Energy Chem.* **2021**, *63*, 594–603. [[CrossRef](#)]
71. Zhang, D.; Yang, K.; Zhang, T.; Luo, M.; Li, M.; Li, Z.; Liu, C.; Ling, Y.; Chen, W.; Zhou, X. A facile “thick to thin” strategy for integrating high volumetric energy density and excellent flexibility into MXene/wood free-standing electrode for supercapacitors. *Chem. Eng. J.* **2023**, *460*, 141733. [[CrossRef](#)]
72. Mashtalir, O.; Naguib, M.; Dyatkin, B.; Gogotsi, Y.; Barsoum, M.W. Kinetics of aluminum extraction from Ti_3AlC_2 in hydrofluoric acid. *Mater. Chem. Phys.* **2013**, *139*, 147–152. [[CrossRef](#)]
73. Wang, X.; Shen, X.; Gao, Y.; Wang, Z.; Yu, R.; Chen, L. Atomic-Scale Recognition of Surface Structure and Intercalation Mechanism of Ti_3C_2X . *J. Am. Chem. Soc.* **2015**, *137*, 2715–2721. [[CrossRef](#)]
74. Halim, J.; Lukatskaya, M.R.; Cook, K.M.; Lu, J.; Smith, C.R.; Näslund, L.-Å.; May, S.J.; Hultman, L.; Gogotsi, Y.; Eklund, P.; et al. Transparent Conductive Two-Dimensional Titanium Carbide Epitaxial Thin Films. *Chem. Mater.* **2014**, *26*, 2374–2381. [[CrossRef](#)] [[PubMed](#)]
75. Xie, X.; Xue, Y.; Li, L.; Chen, S.; Nie, Y.; Ding, W.; Wei, Z. Surface Al leached Ti_3AlC_2 as a substitute for carbon for use as a catalyst support in a harsh corrosive electrochemical system. *Nanoscale* **2014**, *6*, 11035–11040. [[CrossRef](#)] [[PubMed](#)]
76. Li, G.; Tan, L.; Zhang, Y.; Wu, B.; Li, L. Highly Efficiently Delaminated Single-Layered MXene Nanosheets with Large Lateral Size. *Langmuir* **2017**, *33*, 9000–9006. [[CrossRef](#)] [[PubMed](#)]
77. Zhang, B.; Zhu, J.; Shi, P.; Wu, W.; Wang, F. Fluoride-free synthesis and microstructure evolution of novel two-dimensional $Ti_3C_2(OH)_2$ nanoribbons as high-performance anode materials for lithium-ion batteries. *Ceram. Int.* **2019**, *45*, 8395–8405. [[CrossRef](#)]
78. Li, T.; Yao, L.; Liu, Q.; Gu, J.; Luo, R.; Li, J.; Yan, X.; Wang, W.; Liu, P.; Chen, B.; et al. Fluorine-Free Synthesis of High-Purity $Ti_3C_2T_x$ ($T=OH, O$) via Alkali Treatment. *Angew. Chem. Int. Ed.* **2018**, *57*, 6115–6119. [[CrossRef](#)] [[PubMed](#)]
79. Huang, L.; Li, T.; Liu, Q.; Gu, J. Fluorine-free $Ti_3C_2T_x$ as anode materials for Li-ion batteries. *Electrochem. Commun.* **2019**, *104*, 106472. [[CrossRef](#)]

80. Yang, S.; Zhang, P.; Wang, F.; Ricciardulli, A.G.; Lohe, M.R.; Blom, P.W.M.; Feng, X. Fluoride-Free Synthesis of Two-Dimensional Titanium Carbide (MXene) Using A Binary Aqueous System. *Angew. Chem. Int. Ed.* **2018**, *57*, 15491–15495. [[CrossRef](#)]
81. Pang, S.-Y.; Wong, Y.-T.; Yuan, S.; Liu, Y.; Tsang, M.-K.; Yang, Z.; Huang, H.; Wong, W.-T.; Hao, J. Universal Strategy for HF-Free Facile and Rapid Synthesis of Two-dimensional MXenes as Multifunctional Energy Materials. *J. Am. Chem. Soc.* **2019**, *141*, 9610–9616. [[CrossRef](#)] [[PubMed](#)]
82. Li, M.; Lu, J.; Luo, K.; Li, Y.; Chang, K.; Chen, K.; Zhou, J.; Rosen, J.; Hultman, L.; Eklund, P.; et al. Element Replacement Approach by Reaction with Lewis Acidic Molten Salts to Synthesize Nanolaminated MAX Phases and MXene. *J. Am. Chem. Soc.* **2019**, *141*, 4730–4737. [[CrossRef](#)]
83. Li, Y.; Shao, H.; Lin, Z.; Lu, J.; Liu, L.; Duployer, B.; Persson, P.O.Å.; Eklund, P.; Hultman, L.; Li, M.; et al. A general Lewis acidic etching route for preparing MXenes with enhanced electrochemical performance in non-aqueous electrolyte. *Nat. Mater.* **2020**, *19*, 894–899. [[CrossRef](#)]
84. Kamysbayev, V.; Filatov, A.S.; Hu, H.; Rui, X.; Lagunas, F.; Wang, D.; Klie, R.F.; Talapin, D.V. Covalent surface modifications and superconductivity of two-dimensional metal carbide MXenes. *Science* **2020**, *369*, 979–983. [[CrossRef](#)]
85. Gogotsi, Y. Transition metal carbides go 2D. *Nat. Mater.* **2015**, *14*, 1079–1080. [[CrossRef](#)] [[PubMed](#)]
86. Wang, D.; Filatov, A.S.; Cho, W.; Lagunas, F.; Wang, M.; Vaikuntanathan, S.; Liu, C.; Klie, R.F.; Talapin, D.V. Direct synthesis and chemical vapor deposition of 2D carbide and nitride MXenes. *Science* **2023**, *379*, 1242–1247. [[CrossRef](#)]
87. Zhan, C.; Naguib, M.; Lukatskaya, M.; Kent, P.R.C.; Gogotsi, Y.; Jiang, D.-E. Understanding the MXene Pseudocapacitance. *J. Phys. Chem. Lett.* **2018**, *9*, 1223–1228. [[CrossRef](#)] [[PubMed](#)]
88. Xu, X.; Zhang, Y.; Sun, H.; Zhou, J.; Yang, F.; Li, H.; Chen, H.; Chen, Y.; Liu, Z.; Qiu, Z.; et al. Progress and Perspective: MXene and MXene-Based Nanomaterials for High-Performance Energy Storage Devices. *Adv. Electron. Mater.* **2021**, *7*, 2000967. [[CrossRef](#)]
89. Xu, K.; Ji, X.; Zhang, B.; Chen, C.; Ruan, Y.; Miao, L.; Jiang, J. Charging/discharging dynamics in two-dimensional titanium carbide (MXene) slit nanopore: Insights from molecular dynamic study. *Electrochim. Acta* **2016**, *196*, 75–83. [[CrossRef](#)]
90. Lukatskaya, M.R.; Mashtalir, O.; Ren, C.E.; Dall’Agnese, Y.; Rozier, P.; Taberna, P.L.; Naguib, M.; Simon, P.; Barsoum, M.W.; Gogotsi, Y. Cation intercalation and high volumetric capacitance of two-dimensional titanium carbide. *Science* **2013**, *341*, 1502–1505. [[CrossRef](#)]
91. Guan, Y.; Zhao, R.; Cong, Y.; Chen, K.; Wu, J.; Zhu, H.; Dong, Z.; Zhang, Q.; Yuan, G.; Li, Y.; et al. Flexible Ti₂C MXene film: Synthesis, electrochemical performance and capacitance behavior. *Chem. Eng. J.* **2022**, *433*, 133582. [[CrossRef](#)]
92. Guan, Y.; Jiang, S.; Cong, Y.; Wang, J.; Dong, Z.; Zhang, Q.; Yuan, G.; Li, Y.; Li, X. A hydrofluoric acid-free synthesis of 2D vanadium carbide (V₂C) MXene for supercapacitor electrodes. *2D Mater.* **2020**, *7*, 025010. [[CrossRef](#)]
93. Wang, X.; Lin, S.; Tong, H.; Huang, Y.; Tong, P.; Zhao, B.; Dai, J.; Liang, C.; Wang, H.; Zhu, X.; et al. Two-dimensional V₄C₃ MXene as high performance electrode materials for supercapacitors. *Electrochim. Acta* **2019**, *307*, 414–421. [[CrossRef](#)]
94. Xu, T.; Wang, Y.; Liu, K.; Zhao, Q.; Liang, Q.; Zhang, M.; Si, C. Ultralight MXene/carbon nanotube composite aerogel for high-performance flexible supercapacitor. *Adv. Compos. Hybrid Mater.* **2023**, *6*, 108. [[CrossRef](#)]
95. Althubiti, N.A.; Aman, S. Taha Abdel Mohaymen Taha, Synthesis of MnFe₂O₄/MXene/NF nanosized composite for supercapacitor application. *Ceram. Int.* **2023**, *49*, 27496–27505. [[CrossRef](#)]
96. Wang, Y.; Chen, N.; Liu, Y.; Zhou, X.; Pu, B.; Qing, Y.; Zhang, M.; Jiang, X.; Huang, J.; Tang, Q.; et al. MXene/Graphdiyne nanotube composite films for Free-Standing and flexible Solid-State supercapacitor. *Chem. Eng. J.* **2022**, *450*, 138398. [[CrossRef](#)]
97. Zheng, W.; Yang, Y.; Fan, L.; Ye, D.; Xu, W.; Xu, J. Ultralight PPy@PVA/BC/MXene composite aerogels for high-performance supercapacitor electrodes and pressure sensors. *Appl. Surf. Sci.* **2023**, *624*, 157138. [[CrossRef](#)]
98. Mo, T.; Wang, Z.; Zeng, L.; Chen, M.; Kornyshev, A.A.; Zhang, M.; Zhao, Y.; Feng, G. Energy Storage Mechanism in Supercapacitors with Porous Graphdienes: Effects of Pore Topology and Electrode Metallicity. *Adv. Mater.* **2023**, *35*, 2301118. [[CrossRef](#)] [[PubMed](#)]
99. Fan, Z.; Wang, Y.; Xie, Z.; Wang, D.; Yuan, Y.; Kang, H.; Su, B.; Cheng, Z.; Liu, Y. Modified MXene/Holey Graphene Films for Advanced Supercapacitor Electrodes with Superior Energy Storage. *Adv. Sci.* **2018**, *5*, 1800750. [[CrossRef](#)]
100. Li, H.; Chen, R.; Ali, M.; Lee, H.; Ko, M.J. In Situ Grown MWCNTs/MXenes Nanocomposites on Carbon Cloth for High-Performance Flexible Supercapacitors. *Adv. Funct. Mater.* **2020**, *30*, 2002739. [[CrossRef](#)]
101. Zhou, Y.; Maleski, K.; Anasori, B.; Thostenson, J.O.; Pang, Y.; Feng, Y.; Zeng, K.; Parker, C.B.; Zauscher, S.; Gogotsi, Y.; et al. Ti₃C₂T_x MXene-Reduced Graphene Oxide Composite Electrodes for Stretchable Supercapacitors. *ACS Nano* **2020**, *14*, 3576–3586. [[CrossRef](#)] [[PubMed](#)]
102. Ayman, I.; Rasheed, A.; Ajmal, S.; Rehman, A.; Ali, A.; Shakir, I.; Warsi, M.F. CoFe₂O₄ Nanoparticle-Decorated 2D MXene: A Novel Hybrid Material for Supercapacitor Applications. *Energy Fuels* **2020**, *34*, 7622–7630. [[CrossRef](#)]
103. Zhu, Y.; Rajouâ, K.; Le Vot, S.; Fontaine, O.; Simon, P.; Favier, F. MnO₂-MXene Composite as Electrode for Supercapacitor. *J. Electrochem. Soc.* **2022**, *169*, 030524. [[CrossRef](#)]
104. Zhang, X.; Shao, B.; Guo, A.; Sun, Z.; Zhao, J.; Cui, F.; Yang, X. MnO₂ nanoshells/Ti₃C₂T_x MXene hybrid film as supercapacitor electrode. *Appl. Surf. Sci.* **2021**, *560*, 150040. [[CrossRef](#)]
105. Luo, L.; Meng, W.; Wang, G.; Qin, J.; He, H.; Huang, H. MnO₂ nanoflowers-decorated MXene nanosheets with enhanced supercapacitor performance. *J. Alloys Compd.* **2023**, *957*, 170411. [[CrossRef](#)]
106. Prabhakar, N.; Vasanth, S.; Ponpandian, N.; Viswanathan, C. Synthesis effect on surface functionalized Ti₃C₂T_x MXene supported nickel oxide nanocomposites with enhanced specific capacity for supercapacitor application. *J. Energy Storage* **2023**, *72*, 108414.

107. Liu, R.; Zhang, A.; Tang, J.; Tian, J.; Huang, W.; Cai, J.; Barrow, C.; Yang, W.; Liu, J. Fabrication of Cobaltic Oxide Nanoparticle-Doped 3D MXene/Graphene Hybrid Porous Aerogels for All-Solid-State Supercapacitors. *Chem. A Eur. J.* **2019**, *25*, 5547–5554. [[CrossRef](#)] [[PubMed](#)]
108. Wang, Y.; Sun, J.; Qian, X.; Zhang, Y.; Yu, L.; Niu, R.; Zhao, H.; Zhu, J. 2D/2D heterostructures of nickel molybdate and MXene with strong coupled synergistic effect towards enhanced supercapacitor performance. *J. Power Sources* **2019**, *414*, 540–546. [[CrossRef](#)]
109. Xie, W.; Wang, Y.; Zhou, J.; Zhang, M.; Yu, J.; Zhu, C.; Xu, J. MOF-derived CoFe₂O₄ nanorods anchored in MXene nanosheets for all pseudocapacitive flexible supercapacitors with superior energy storage. *Appl. Surf. Sci.* **2020**, *534*, 147584. [[CrossRef](#)]
110. Zhou, H.; Wu, F.; Fang, L.; Hu, J.; Luo, H.; Guan, T.; Hu, B.; Zhou, M. Layered NiFe-LDH/MXene nanocomposite electrode for high-performance supercapacitor. *Int. J. Hydrogen Energy* **2020**, *45*, 13080–13089. [[CrossRef](#)]
111. Liang, C.; Feng, Z.; Chen, M.; Xu, X.; Lu, M.; Wang, W. Nanoflower-like hollow NiMnCo-OH decorated with self-assembled 2D Ti₃C₂T_x for high-efficiency hybrid supercapacitors. *J. Alloys Compd.* **2024**, *970*, 172537. [[CrossRef](#)]
112. Wang, X.; Wang, Y.; Liu, D.; Li, X.; Xiao, H.; Ma, Y.; Xu, M.; Yuan, G.; Chen, G. Opening MXene Ion Transport Channels by Intercalating PANI Nanoparticles from the Self-Assembly Approach for High Volumetric and Areal Energy Density Supercapacitors. *ACS Appl. Mater. Interfaces* **2021**, *13*, 30633–30642. [[CrossRef](#)] [[PubMed](#)]
113. Wu, W.; Niu, D.; Zhu, J.; Gao, Y.; Wei, D.; Liu, X.; Wang, F.; Wang, L.; Yang, L. Organ-like Ti₃C₂ MXenes/polyaniline composites by chemical grafting as high-performance supercapacitors. *J. Electroanal. Chem.* **2019**, *847*, 113203. [[CrossRef](#)]
114. Pathak, I.; Acharya, D.; Chhetri, K.; Lohani, P.C.; Ko, T.H.; Muthurasu, A.; Subedi, S.; Kim, T.; Saidin, S.; Dahal, B.; et al. Ti₃C₂T_x MXene integrated hollow carbon nanofibers with polypyrrole layers for MOF-derived freestanding electrodes of flexible asymmetric supercapacitors. *Chem. Eng. J.* **2023**, *469*, 143388. [[CrossRef](#)]
115. Kosnan, M.A.; Asyadi, A.M.; Ezyanie, S.N.; Farahiyan, M.R.; Akito, T. Recent Progress of Electrode Architecture for MXene/MoS₂ Supercapacitor: Preparation Methods and Characterizations. *Micromachines* **2022**, *13*, 1837. [[CrossRef](#)]
116. Hussain, S.; Iqra, R.; Dhanasekaran, V.; Taqi, M.; Faisal, S.; Soo, S.Y.; Seok, K.H.; Jongwan, J. Designing the MXene/molybdenum diselenide hybrid nanostructures for high-performance symmetric supercapacitor and hydrogen evolution applications. *Int. J. Energy Res.* **2021**, *45*, 18770. [[CrossRef](#)]
117. Arulkumar, C.; Gandhi, R.; Vadivel, S. Ultra-thin nanosheets of Ti₃C₂T_x MXene/MoS₂ nanocomposite electrode for asymmetric supercapacitor and electrocatalytic water splitting. *Electrochim. Acta* **2023**, *462*, 142742. [[CrossRef](#)]
118. Chandran, M.; Anitta, T.; Asha, R.; Mari, V.; Bhagiyalakshmi, M. MoS₂ Confined MXene Heterostructures as Electrode Material for Energy Storage Application. *J. Energy Storage* **2020**, *30*, 101446. [[CrossRef](#)]
119. Chen, X.; Zhu, J.; Cai, J.; Zhang, Y.; Wang, X. Nanosheets assembled layered MXene/MoS₂ nanohybrid positive electrode materials for high-performance asymmetric supercapacitors. *J. Energy Storage* **2021**, *40*, 102721. [[CrossRef](#)]
120. Sharma, A.; Rout, C.S. 1T metallic vanadium disulfide hybridized with MXene and functionalized-MWCNT as a remarkable electrode for high power density asymmetric supercapacitor applications. *Int. J. Energy Res.* **2022**, *46*, 24537–24553. [[CrossRef](#)]
121. Mao, K.; Shi, J.; Zhang, Q.; Hou, Y.; Wen, L.; Liu, Z.; Long, F.; Niu, K.; Liu, N.; Long, F.; et al. High-capacitance MXene anode based on Zn-ion pre-intercalation strategy for degradable micro Zn-ion hybrid supercapacitors. *Nano Energy* **2022**, *103*, 107791. [[CrossRef](#)]
122. Javed, M.S.; Zhang, X.; Ali, S.; Mateen, A.; Idrees, M.; Sajjad, M.; Batool, S.; Ahmad, A.; Imran, M.; Najam, T.; et al. Heterostructured bimetallic-sulfide@layered Ti₃C₂T-MXene as a synergistic electrode to realize high-energy-density aqueous hybrid-supercapacitor. *Nano Energy* **2022**, *101*, 107624. [[CrossRef](#)]
123. Zheng, Z.; Wu, W.; Yang, T.; Wang, E.; Du, Z.; Hou, X.; Liang, T. In situ reduced MXene/AuNPs composite toward enhanced charging/discharging and specific capacitance. *J. Adv. Ceram.* **2021**, *10*, 1061–1071. [[CrossRef](#)]
124. Li, L.; Niu, H.; Robertson, J.; Jiang, Z.; Guo, Y.; Kuai, C. Cyclocrosslinked polyphosphazene modified MXene as aqueous supercapacitor. *Electrochim. Acta* **2023**, *439*, 141574. [[CrossRef](#)]
125. Jia, B.; Yang, H.; Wang, L.; Zhao, Z.; Wu, X. Synergistic interface-pillared Fe-MOF on 2D Ti₃C₂T_x MXene electrode coupling toward high energy density. *Appl. Surf. Sci.* **2022**, *602*, 154386. [[CrossRef](#)]
126. Xu, H.; Fan, J.; Su, H.; Liu, C.; Chen, G.; Dall’Agnese, Y.; Gao, Y. Metal Ion-Induced Porous MXene for All-Solid-State Flexible Supercapacitors. *Nano Lett.* **2023**, *23*, 283–290. [[CrossRef](#)]
127. Li, K.; Wang, X.; Li, S.; Urbankowski, P.; Li, J.; Xu, Y.; Gogotsi, Y. An Ultrafast Conducting Polymer@MXene Positive Electrode with High Volumetric Capacitance for Advanced Asymmetric Supercapacitors. *Small* **2020**, *16*, 1906851. [[CrossRef](#)]
128. Fu, J.; Yun, J.; Wu, S.; Li, L.; Yu, L.; Kim, K.H. Architecturally Robust Graphene-Encapsulated MXene Ti₂CT_x@Polyaniline Composite for High-Performance Pouch-Type Asymmetric Supercapacitor. *ACS Appl. Mater. Interfaces* **2018**, *10*, 34212–34221. [[CrossRef](#)] [[PubMed](#)]
129. Zhao, K.; Wang, H.; Zhu, C.; Lin, S.; Xu, Z.; Zhang, X. Free-standing MXene film modified by amorphous FeOOH quantum dots for high-performance asymmetric supercapacitor. *Electrochim. Acta* **2019**, *308*, 1–8. [[CrossRef](#)]
130. Xia, Q.X.; Fu, J.; Yun, J.M.; Mane, R.S.; Kim, K.H. High volumetric energy density annealed-MXene-nickel oxide/MXene asymmetric supercapacitor. *RSC Adv.* **2017**, *7*, 11000–11011. [[CrossRef](#)]
131. Wang, Y.; Wang, X.; Li, X.; Bai, Y.; Xiao, H.; Liu, Y.; Yuan, G. Scalable fabrication of polyaniline nanodots decorated MXene film electrodes enabled by viscous functional inks for high-energy-density asymmetric supercapacitors. *Chem. Eng. J.* **2021**, *405*, 126664. [[CrossRef](#)]

132. Li, L.; Zhang, N.; Zhang, M.; Zhang, X.; Zhang, Z. Flexible $\text{Ti}_3\text{C}_2\text{T}_x$ /PEDOT:PSS films with outstanding volumetric capacitance for asymmetric supercapacitors. *Dalton Trans.* **2019**, *48*, 1747–1756. [[CrossRef](#)] [[PubMed](#)]
133. Jian, X.; He, M.; Chen, L.; Zhang, M.M.; Li, R.; Gao, L.J.; Fu, F.; Liang, Z.-H. Three-dimensional carambola-like MXene/polypyrrole composite produced by one-step co-electrodeposition method for electrochemical energy storage. *Electrochim. Acta* **2019**, *318*, 820–827. [[CrossRef](#)]
134. Tong, L.; Jiang, C.; Cai, K.; Wei, P. High-performance and freestanding PPy/ $\text{Ti}_3\text{C}_2\text{T}_x$ composite film for flexible all-solid-state supercapacitors. *J. Power Sources* **2020**, *465*, 228267. [[CrossRef](#)]
135. Li, Y.; Kamdem, P.; Jin, X.J. Hierarchical architecture of MXene/PANI hybrid electrode for advanced asymmetric supercapacitors. *J. Alloys Compd.* **2021**, *850*, 156608. [[CrossRef](#)]
136. Qin, L.; Tao, Q.; El Ghazaly, A.; Fernandez-Rodriguez, J.; Persson, P.O.; Rosen, J.; Zhang, F. High-Performance Ultrathin Flexible Solid-State Supercapacitors Based on Solution Processable $\text{Mo}_{1.33}\text{C}$ MXene and PEDOT:PSS. *Adv. Funct. Mater.* **2018**, *28*, 1703808. [[CrossRef](#)]
137. Xia, Q.X.; Shinde, N.M.; Zhang, T.; Yun, J.M.; Zhou, A.; Mane, R.S.; Mathur, S.; Kim, K.H. Seawater electrolyte-mediated high volumetric MXene-based electrochemical symmetric supercapacitors. *Dalton Trans.* **2018**, *47*, 8676–8682. [[CrossRef](#)]
138. Zhu, K.; Jin, Y.; Du, F.; Gao, S.; Gao, Z.; Meng, X.; Chen, G.; Wei, Y.; Gao, Y. Synthesis of Ti_2CT_x MXene as electrode materials for symmetric supercapacitor with capable volumetric capacitance. *J. Energy Chem.* **2019**, *31*, 11–18. [[CrossRef](#)]
139. Wang, J.; Gong, J.; Zhang, H.; Lv, L.; Liu, Y.; Dai, Y. Construction of hexagonal nickel-cobalt oxide nanosheets on metal-organic frameworks based on MXene interlayer ion effect for hybrid supercapacitors. *J. Alloys Compd.* **2021**, *870*, 159466. [[CrossRef](#)]
140. Guo, Z.; Li, Y.; Lu, Z.; Chao, Y.; Liu, W. High-performance MnO_2 @MXene/carbon nanotube fiber electrodes with internal and external construction for supercapacitors. *J. Mater. Sci.* **2022**, *57*, 3613–3628. [[CrossRef](#)]
141. Jiang, H.; Wang, Z.; Yang, Q.; Hanif, M.; Wang, Z.; Dong, L.; Dong, M. A novel MnO_2 / $\text{Ti}_3\text{C}_2\text{T}_x$ MXene nanocomposite as high performance electrode materials for flexible supercapacitors. *Electrochim. Acta* **2018**, *290*, 695–703. [[CrossRef](#)]
142. Shen, B.; Liao, X.; Zhang, X.; Ren, H.T.; Lin, J.H.; Lou, C.W.; Li, T.T. Synthesis of Nb₂C MXene-based 2D layered structure electrode material for high-performance battery-type supercapacitors. *Electrochim. Acta* **2022**, *413*, 140144. [[CrossRef](#)]
143. Zhang, Y.; Cao, J.; Yuan, Z.; Zhao, L.; Wang, L.; Han, W. Assembling Co_3O_4 Nanoparticles into MXene with Enhanced electrochemical performance for advanced asymmetric supercapacitors. *J. Colloid Interface Sci.* **2021**, *599*, 109–118. [[CrossRef](#)] [[PubMed](#)]
144. Mahmood, M.; Chaudhary, K.; Shahid, M.; Shakir, I.; Agboola, P.O.; Aadil, M. Fabrication of MoO_3 Nanowires/MXene@CC hybrid as highly conductive and flexible electrode for next-generation supercapacitors applications. *Ceram. Int.* **2022**, *48*, 19314–19323. [[CrossRef](#)]
145. Liu, H.; Hu, R.; Qi, J.; Sui, Y.; He, Y.; Meng, Q.; Wei, F.; Ren, Y.; Ren, Y.; Wei, W. One-Step Synthesis of Nanostructured CoS_2 Grown on Titanium Carbide MXene for High-Performance Asymmetrical Supercapacitors. *Adv. Mater. Interfaces* **2020**, *7*, 1901659. [[CrossRef](#)]
146. Liu, Y.; Gong, J.; Wang, J.; Hu, C.; Xie, M.; Jin, X.; Wang, S.; Dai, Y. Facile fabrication of MXene supported nickel-cobalt selenide ternary composite via one-step hydrothermal for high-performance asymmetric supercapacitors. *J. Alloys Compd.* **2022**, *899*, 163354. [[CrossRef](#)]
147. Zhang, X.; Yang, S.; Lu, W.; Lei, D.; Tian, Y.; Guo, M.; Mi, P.; Qu, N.; Zhao, Y. MXenes induced formation of Ni-MOF microbelts for high-performance supercapacitors. *J. Colloid Interface Sci.* **2021**, *592*, 95–102. [[CrossRef](#)] [[PubMed](#)]
148. Li, C.; Wang, S.; Cui, Y.; Wang, X.; Yong, Z.; Liang, D.; Chi, Y.; Wang, Z. Sandwich-like high-load MXene/polyaniline film electrodes with ultrahigh volumetric capacitance for flexible supercapacitors. *J. Colloid Interface Sci.* **2022**, *620*, 35–46. [[CrossRef](#)] [[PubMed](#)]
149. Xu, H.; Cui, L.; Lei, Z.; Xu, M.; Jin, X. MXene/carboxymethylcellulose-polyaniline ($\text{Ti}_3\text{C}_2\text{T}_x$ /CMC-PANI) film as flexible electrode for high-performance asymmetric supercapacitors. *Electrochim. Acta* **2022**, *436*, 141408. [[CrossRef](#)]
150. Chen, Z.; Wang, Y.; Han, J.; Wang, T.; Leng, Y.; Wang, Y.; Li, T.; Han, Y. Preparation of Polyaniline onto dl-Tartaric Acid Assembled MXene Surface as an Electrode Material for Supercapacitors. *ACS Appl. Energy Mater.* **2020**, *3*, 9326–9336. [[CrossRef](#)]
151. Murali, S.; Quarles, N.; Zhang, L.L.; Potts, J.R.; Tan, Z.; Lu, Y.; Zhu, Y.; Ruoff, R.S. Volumetric capacitance of compressed activated microwave-expanded graphite oxide (a-MEGO) electrodes. *Nano Energy* **2013**, *2*, 764–768. [[CrossRef](#)]
152. Gao, Y.; Wang, L.; Li, Z.; Zhang, Y.; Xing, B.; Zhang, C.; Zhou, A. Electrochemical performance of Ti_3C_2 supercapacitors in KOH electrolyte. *J. Adv. Ceram.* **2015**, *4*, 130–134. [[CrossRef](#)]
153. Lukatskaya, M.R.; Kota, S.; Lin, Z.; Zhao, M.-Q.; Shpigel, N.; Levi, M.D.; Halim, J.; Taberna, P.-L.; Barsoum, M.W.; Simon, P. Ultra-high-rate pseudocapacitive energy storage in two-dimensional transition metal carbides. *Nat. Energy* **2017**, *2*, 17105. [[CrossRef](#)]
154. Wang, X.; Mathis, T.S.; Li, K.; Lin, Z.; Vlcek, L.; Torita, T.; Osti, N.C.; Hatter, C.; Urbankowski, P.; Sarycheva, A. Influences from solvents on charge storage in titanium carbide MXenes. *Nat. Energy* **2019**, *4*, 241–248. [[CrossRef](#)]
155. Liu, C.; Wu, H.; Wang, X.; Fan, J.; Su, H.; Yang, D.; Wei, Y.; Du, F.; Dall, Y.; Gao, Y. Flexible solid-state supercapacitor integrated by methanesulfonic acid/polyvinyl acetate hydrogel and $\text{Ti}_3\text{C}_2\text{T}_x$. *Energy Storage Mater.* **2023**, *54*, 164–171. [[CrossRef](#)]
156. Hui, X.; Ge, X.; Zhao, R.; Li, Z.; Yin, L. Interface chemistry on MXene-based materials for enhanced energy storage and conversion performance. *Adv. Funct. Mater.* **2020**, *30*, 2005190. [[CrossRef](#)]

157. Hu, M.; Hu, T.; Cheng, R.; Yang, J.; Cui, C.; Zhang, C.; Wang, X. MXene-coated silk-derived carbon cloth toward flexible electrode for supercapacitor application. *J. Energy Chem.* **2018**, *27*, 161–166. [[CrossRef](#)]
158. Gao, Z.W.; Zheng, W.; Lee, L.Y.S. Highly enhanced pseudocapacitive performance of vanadium-doped MXenes in neutral electrolytes. *Small* **2019**, *15*, 1902649. [[CrossRef](#)] [[PubMed](#)]
159. Tian, Y.; Yang, C.; Luo, Y.; Zhao, H.; Du, Y.; Kong, L.B.; Que, W. Understanding MXene-based “symmetric” supercapacitors and redox electrolyte energy storage. *ACS Appl. Energy Mater.* **2020**, *3*, 5006–5014. [[CrossRef](#)]
160. Mu, X.; Wang, D.; Du, F.; Chen, G.; Wang, C.; Wei, Y.; Gogotsi, Y.; Gao, Y.; Dall, Y. Revealing the pseudo-intercalation charge storage mechanism of MXenes in acidic electrolyte. *Adv. Funct. Mater.* **2019**, *29*, 1902953. [[CrossRef](#)]
161. Luo, J.; Fang, C.; Jin, C.; Yuan, H.; Sheng, O.; Fang, R.; Zhang, W.; Huang, H.; Gan, Y.; Xia, Y. Tunable pseudocapacitance storage of MXene by cation pillaring for high performance sodium-ion capacitors. *J. Mater. Chem. A* **2018**, *6*, 7794–7806. [[CrossRef](#)]
162. Shao, H.; Lin, Z.; Xu, K.; Taberna, P.-L.; Simon, P. Electrochemical study of pseudocapacitive behavior of $\text{Ti}_3\text{C}_2\text{T}_x$ MXene material in aqueous electrolytes. *Energy Storage Mater.* **2019**, *18*, 456–461. [[CrossRef](#)]
163. Allah, A.E.; Wang, J.; Kaneti, Y.V.; Li, T.; Farghali, A.A.; Khedr, M.H.; Nanjundan, A.K.; Ding, B.; Dou, H.; Zhang, X.; et al. Auto-programmed heteroarchitecturing: Self-assembling ordered mesoporous carbon between two-dimensional $\text{Ti}_3\text{C}_2\text{T}_x$ MXene layers. *Nano Energy* **2019**, *65*, 103991. [[CrossRef](#)]
164. Li, H.; Chen, X.; Zalnezhad, E.; Hui, K.N.; Hui, K.S.; Ko, M.J. 3D hierarchical transition-metal sulfides deposited on MXene as binder-free electrode for high-performance supercapacitors. *J. Ind.* **2020**, *82*, 309–316. [[CrossRef](#)]
165. Zhao, M.Q.; Ren, C.E.; Ling, Z.; Lukatskaya, M.R.; Zhang, C.; Van Aken, K.L.; Barsoum, M.W.; Barsoum, Y. Flexible MXene/carbon nanotube composite paper with high volumetric capacitance. *Adv. Mater.* **2014**, *27*, 0935–9648. [[CrossRef](#)] [[PubMed](#)]
166. Yan, J.; Ren, C.E.; Maleski, K.; Hatter, C.B.; Anasori, B.; Urbankowski, P.; Sarycheva, A.; Gogotsi, Y. Flexible MXene/graphene films for ultrafast supercapacitors with outstanding volumetric capacitance. *Adv. Funct. Mater.* **2017**, *27*, 1701264. [[CrossRef](#)]
167. Zhu, M.; Huang, Y.; Deng, Q.; Zhou, J.; Pei, Z.; Xue, Q.; Huang, Y.; Wang, Z.; Li, H.; Huang, Q. Highly flexible freestanding supercapacitor electrode with enhanced performance obtained by hybridizing polypyrrole chains with MXene. *Adv. Energy Mater.* **2016**, *6*, 1600969. [[CrossRef](#)]

Disclaimer/Publisher’s Note: The statements, opinions and data contained in all publications are solely those of the individual author(s) and contributor(s) and not of MDPI and/or the editor(s). MDPI and/or the editor(s) disclaim responsibility for any injury to people or property resulting from any ideas, methods, instructions or products referred to in the content.